Deepening roots can enhance carbonate weathering

Hang Wen[1], Pamela L. Sullivan[2], Gwendolyn L. Macpherson[3], Sharon A. Billings[4], Li Li[1]

[1] Department of Civil and Environmental Engineering, Pennsylvania State University, University Park PA 16802, United States

[2] College of Earth, Ocean, and Atmospheric Science, Oregon State University, Corvallis OR 97331, United States

5   [3] Department of Geology, University of Kansas, Lawrence KS 66045, United States

[4] Department of Ecology and Evolutionary Biology and Kansas Biological Survey, University of Kansas, Lawrence KS 66045, United States

Correspondence to: Li Li (lili@engr.psu.edu)

Abstract: Carbonate weathering is essential in regulating atmospheric CO_2 and carbon cycle at the century time scale. Plant roots
10   have been known to accelerate weathering by elevating soil CO_2 via respiration. It however remains poorly understood how and how much rooting characteristics (e.g., depth and density distribution) modify flow paths and weathering. We address this knowledge gap using field data from and reactive transport numerical experiments at the Konza Prairie Biological Station (Konza), Kansas (USA), a site where woody encroachment into grasslands is surmised to deepen roots.

Results indicate that deepening roots potentially enhance weathering in two ways. First, deepening roots can control
15   thermodynamic limits of carbonate dissolution by regulating how much CO_2 transports downward to the deeper carbonate-rich zone. The base-case data and model from Konza reveal that concentrations of Ca and Dissolved Inorganic Carbon (DIC) are regulated by soil $p$$CO_2$ driven by the seasonal fluctuation of soil respiration. This relationship can be encapsulated in equations derived in this work describing the dependence of Ca and DIC on temperature and soil CO_2, which has been shown to apply in multiple carbonate-dominated catchments. Second, numerical experiments show that roots control weathering rates by regulating
20   the amount of water fluxes that flush through the carbonate zone and export reaction products at dissolution equilibrium. Numerical experiments explored the potential effects of partitioning 40% of infiltrated water to depth in woodlands compared to 5% in grasslands. Soil CO_2 data from wood- and grasslands suggest relatively similar soil CO_2 distribution over depth, and only led to 1% to 12% difference in weathering rates if flow partitioning was kept the same between the two land covers. In contrast, deepening roots can enhance weathering by 17% to 207% as infiltration rates increased from 3.7×10^{-2} to 3.7 m/yr. Numerical experiments
25   also indicated that weathering fronts in woodlands propagated > 2 times deeper compared to grasslands after 300 years at the infiltration rate of 0.37 m/yr. These differences in weathering fronts are ultimately caused by the contact time of CO_2-charged water with carbonate rocks. We recognize that modeling results are subject to limitations in representing processes and parameters, but we propose that the data and numerical experiments allude to the hypothesis that 1) deepening roots can enhance carbonate weathering; 2) the hydrological impacts of rooting characteristics can be more influential than those of soil CO_2 distribution in
30   modulating weathering rates. We call for co-located characterizations of roots, subsurface structure, soil CO_2 levels, and their linkage to water and water chemistry. These measurements will be essential to improve models and illuminate feedback mechanisms of land cover changes, chemical weathering, global carbon cycle, and climate.

1 Introduction

About 7–12% of the Earth's continental area is carbonate based; about 25% of the global population completely or
35   partially depend on waters from karst aquifers (Hartmann et al., 2014). Carbonate weathering has long been considered negligible as a long-term control of atmospheric CO_2 (0.5 to 1 Myr; (Berner and Berner, 2012;Winnick and Maher, 2018). Recent studies

however have underscored its significance in controlling global carbon cycle at the century time scale that is relevant to modern climate change, owing to its rapid dissolution, fast response to perturbations, and the order of magnitude higher carbon store in carbonate reservoirs compared to the atmosphere (Gaillardet et al., 2019). Carbonate weathering is influenced by many factors,

40 including temperature (Romero-Mujalli et al., 2019b), hydrological regimes (Romero-Mujalli et al., 2019a;Wen and Li, 2018), and soil CO_2 concentrations (Covington et al., 2015) arising from vegetation type (Calmels et al., 2014). Rapid alteration to any of these factors, either human or climate induced, may change global carbonate weathering fluxes and lead to a departure from the current global atmospheric CO_2 level.

Plant roots have long been recognized as a dominant biotic-driver of chemical weathering and global carbon cycle (Berner,

45 1992;Beerling et al., 1998;Brantley et al., 2017a). The growth of forests has been documented to elevate soil pCO_2 and amplify Dissolved Inorganic Carbon (DIC) fluxes (Berner, 1997;Andrews and Schlesinger, 2001). Rooting structure can influence weathering in two ways. First, rooting systems (e.g., grass-, shrub- and woodlands) may affect the distribution of soil carbon (both organic and inorganic), microbe biomass, and soil respiration at depth (Drever, 1994;Jackson et al., 1996;Billings et al., 2018). The relatively deep root distributions of shrublands compared to grasslands may lead to deeper soil carbon profiles (Jackson et al.,

50 1996;Jobbagy and Jackson, 2000), which may help elevate CO_2 and acidity that determine carbonate solubility and weathering rates.

Second, plant roots may affect soil structure and hydrological processes. Root trenching and etching can develop porosity (Mottershead et al., 2003;Hasenmueller et al., 2017). Root death and decay can promote the generation of macropores, or more specifically, biopores with connected networks (Angers and Caron, 1998;Zhang et al., 2015). Root channels have been estimated

55 to account for about 70% of the total described macropores (Noguchi et al., 1997;Beven and Germann, 2013) and for >70% of water fluxes through soils (Watson and Luxmoore, 1986). In grasslands, the lateral, dense spread of roots in top soils promote horizontal macropores that support near-surface, lateral flow (Cheng et al., 2011). Highly dense fine roots also increase the abundance of organic matter and promote granular or "sandy" texture soil aggregates that facilitate shallow, near-surface water flow (Oades, 1993;Nippert et al., 2012). In contrast, shrublands and forests with deep and thick roots tend to have a high proportion

60 of macropores and high connectivity to the deep subsurface (Canadell et al., 1996;Nardini et al., 2016), enhancing the drainage of water to the depth (Pawlik et al., 2016).

It is generally known that rooting characteristics vary among plant species and are critical in regulating flow paths and storage (Nepstad et al., 1994;Jackson et al., 1996;Cheng et al., 2011;Brunner et al., 2015;Fan et al., 2017). Existing studies however have primarily focused on the role of soil CO_2 and organic acids (Drever, 1994;Lawrence et al., 2014;Gaillardet et al., 2019).

65 Systematic studies on coupled effects of flow partitioning and soil CO_2 distribution are missing, owing to the limitation in data that detail rooting effects on flow partitioning and complex hydrological-biogeochemical interactions. Here we ask the questions: how and to what degree do rooting characteristics influence carbonate weathering when considering both flow partitioning and soil CO_2 distribution? Which factor (flow partitioning or soil CO_2 distribution) predominantly controls weathering? We hypothesized that deepening roots in woodlands enhance carbonate weathering by promoting deeper recharge and CO_2-carbonate

70 contact at depth (Figure 1).

We tested the hypotheses by a series of numerical experiments integrating reactive transport modelling and water chemistry data from an upland watershed in the Konza Prairie Biological Station, a tallgrass prairie and one of the Long-Term Ecological Research (LTER) sites in the US (Figure S1). We used the calibrated model to carry out numerical experiments for two end-members of vegetation covers, grasslands and woodlands, under flow-partitioning conditions that are characteristic of their

75 rooting structure. These experiments differentiated the impact of biogeochemical and hydrological drivers and bracketed the range

of their potential impacts on weathering, thus providing insights on the missing quantitative link between rooting structure, flow paths, and chemical weathering.

2 Research site and data sources

Site description. Details of the Konza site are in the Supporting Information (SI) and references therein. Here we provide brief information most relevant to this work. Konza is a mesic native grassland where experimentally manipulated, long-term burning regimes have led to woody encroachment in up to 70% of the catchment area in some catchments. The mean annual temperature and precipitation are 13°C and ~ 835 mm, respectively (Tsypin and Macpherson, 2012). The bedrock contains repeating Permian couplets of limestone (1-2 m thick) and mudstone (2-4 m) (Macpherson et al., 2008). The limestone is primarily calcite with traces of dolomite while the mudstone is dominated by illite, chlorite, and mixed-layers of chlorite-illite and chlorite-vermiculite, varying in abundance from major to trace amounts. With an average thickness of 1-2 m in the lowlands, soils mostly have carbonate less than 25% (Macpherson et al., 2008). Data suggest that the Konza landscape is undergoing a hydrogeochemical transition that coincides with and may be driven by woody-encroachment. In parallel to these changes is a detectable decline in stream flow and an increase in weathering rates (Macpherson and Sullivan, 2019) and groundwater pCO$_2$ (Macpherson et al., 2008). Stream water concentration-discharge (C-Q) patterns have exhibited chemodynamic patterns (i.e., solute concentrations are sensitive to changes in discharge) for geogenic species (e.g., Mg and Na) in woody-encroached sites compared to grass sites. Sullivan et al. (2019) hypothesized that concentration-discharge relationships may be affected by woody species with deeper roots, which altered flow paths and mineral-water interactions (Figure 1). We focus on the upland watershed N04d in Konza (Figure S1) that has experienced a 4-year burning interval since 1990 and has seen considerable woody encroachment and changes in hydrologic fluxes (Sullivan et al., 2019).

Data sources. Daily total meteoric precipitation and evapotranspiration were from the Konza data website (*lter.konza.ksu.edu/data*). Wet chemistry deposition data was from the National Atmospheric Deposition Program NADP (*nadp.sws.uiuc.edu*). Monthly data of soil gases (16, 84 and 152 cm), soil water (17 and 152 cm), and groundwater (366 cm) from 2009-2010 were used for this work (Tsypin and Macpherson, 2012) (Figure 2A). The sampling points were about 30 m away from the stream. More information on field and laboratory methods were included in the SI.
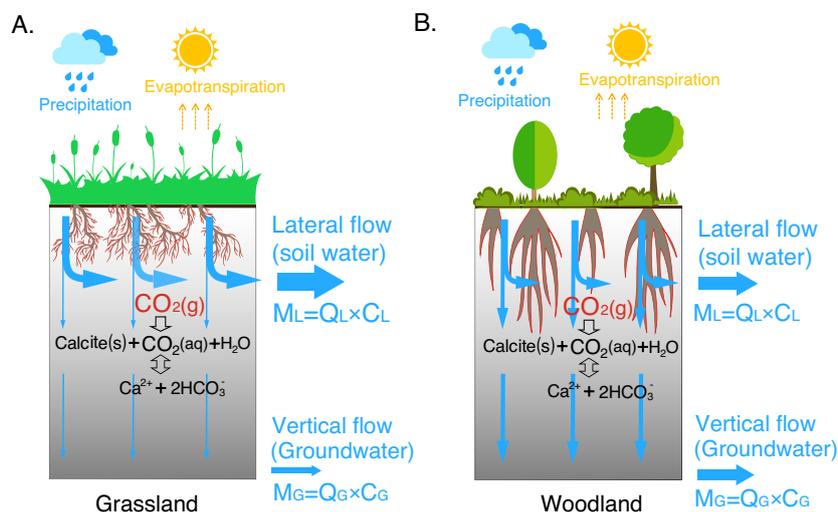
Figure 1. A conceptual diagram of hydro-biogeochemical interactions in the grassland (A) and woodland (B). The shallow and dense fine roots in the grassland promotes lateral macropore development and lateral water flow; the deeper roots in the woodland induces vertical macropore development that supports vertical flow into groundwater. The gray color gradient reflects the calcite abundance with more calcite in depth. M_L and M_G with a unit of mol/yr (= flow rate Q (m/yr) $\times$ species concentration C (mol/m³) $\times$ unit cross-section area (m²)) represent mass fluxes from lateral flow (soil water) and from vertical flow into groundwater, respectively. Soil water and groundwater were assumed to eventually flow into stream. Infiltration rate $Q_T = Q_L + Q_G$.

3 Reactive transport modeling

3.1 Base case: 1D reactive transport model for the Konza grassland (calibrated with field data)

A 1-D reactive transport model was developed using the code CrunchTope (Steefel et al., 2015). The code solves mass conservation equations integrating advective and diffusive / dispersive transport and geochemical reactions. It has been extensively used in understanding mineral dissolution, chemical weathering, and biogeochemical reactions (e.g., Lawrence et al. (2014);Wen et al. (2016); Deng et al. (2017)). In this study, the base case had a porosity of 0.48 and a depth of 366.0 cm at a resolution 1.0 cm. Soil temperature was assumed to decrease linearly from 17 °C at the land surface to 8°C at 366.0 cm, within typical ranges of field measurements (Tsypin and Macpherson, 2012). Detailed set up of domain, soil mineralogy, initial condition, and precipitation chemistry, are in the SI.

Representation of soil CO₂. The model does not explicitly simulate soil respiration (microbial activities and root respiration) that produces soil CO₂. Instead, it approximates these processes by having a solid phase "CO₂(g*)" that continuously releases CO₂(g) that dissolves into CO₂(aq) (and other relevant aqueous species) at a kinetic rate constant of 10^{-9} mol/m²/s (Reaction 0-1 in Table 1) that reproduced the observed soil pCO₂ levels. This value is at the low end of the reported soil respiration rates ($10^{-9} \sim 10^{-5}$ mol/m²/s) (Bengtson and Bengtsson, 2007;Ahrens et al., 2015;Carey et al., 2016). The dissolution of CO₂(g*) via CO₂(g) into CO₂(aq) follows Henry's law $C_{CO_2(aq)} = K_1 pCO_2$. Here K_1 is the equilibrium constant of Reaction 1, essentially Henry's law constant. The extent of CO₂(g*) dissolution (i.e., the mass change of the solid phase over time) was constrained by $C_{CO_2(aq)}$, which was estimated using temperature-dependent K_1 (following the van't Hoff equation in Eq. S1) and measured soil CO₂ data at different horizons (Table 2). These $C_{CO_2(aq)}$ values were then linearly interpolated for individual grid blocks in the model. Finally, these

prescribed $C_{CO_2(aq)}$ values were used as the equilibrium constants of the coupled Reaction 0-1 in the form of $CO_2(g^*) \leftrightarrow CO_2(aq)$, such that the soil CO_2 at different depth were represented (Section 4.1). In the base case, the soil profile of $C_{CO_2(aq)}$ values were updated monthly based on the monthly soil CO_2 data (Table 2). More details about the implementation in CrunchTope are included

130 in the SI.

Table 1. Key reactions and kinetic and thermodynamic parameters

Reaction	$\log_{10}K_{eq}$ at 25 °C[a]	Standard enthalpy ($\Delta H°$, kJ/mol)	$\log_{10}k$ (mol/m²/s) at 25 °C [d]	Specific Surface Area (m²/g)[d]
Soil CO_2 production through $CO_2(g^*)$ and dissolving into $CO_2(aq)$				
(0) $CO_2(g^*) \leftrightarrow CO_2(g)$	-	-	-9.00	1.0
(1) $CO_2(g) \leftrightarrow CO_2(aq)$	-1.46[b]	-19.98	-	-
(2) $CO_2(aq) + H_2O \leftrightarrow H^+ + HCO_3^-$	-6.35	9.10	-	-
(3) $HCO_3^- \leftrightarrow H^+ + CO_3^{2-}$	-10.33	14.90	-	-
Chemical weathering				
(4) $CaCO_3(s) + CO_2(aq) + H_2O \leftrightarrow Ca^{2+} + 2HCO_3^-$	-5.12[c] -4.52[c]	-15.41	-6.69	0.84
[e](5) $CaAl_2Si_2O_8(s) + 8H^+ \leftrightarrow Ca^{2+} + 2Al^{3+} + 2H_4SiO_4(aq)$	26.58	-	-11.00	0.045
[e](6) $KAlSi_3O_8(s) + 4H^+ + 4H_2O \leftrightarrow Al^{3+} + K^+ + 3H_4SiO_4(aq)$	-0.28	-	-12.41	0.20
[e](7) $Al_2Si_2O_5(OH)_4(s) + 6H^+ \leftrightarrow 2Al^{3+} + 2H_4SiO_4(aq) + H_2O$	6.81	-	-12.97	17.50

a. Values of K_{eq} were interpolated using the EQ3/6 database (Wolery et al., 1990), except Reaction 1 and 4 (i.e., K_1 and K_4).
b. By combining the temporal- and spatial-dependent soil pCO₂ data, CO₂(aq) concentrations were calculated through $C_{CO_2(aq)} = K_1pCO_2$. The prescribed $C_{CO_2(aq)}$ values were used as equilibrium constants in CrunchTope to describe how much soil CO₂
135   was available for weathering.
c. Calcite in the shallow soil (above Horizon B) is mixed with other minerals and has small particle size (Macpherson and Sullivan, 2019), relatively "impure" and therefore has a lower K_{eq} value than those at depth with relatively "pure" calcite. The K_{eq} of the "impure" calcite was calibrated by fitting field data of Ca and alkalinity.
d. The kinetic rate parameters and specific surface areas were from Palandri and Kharaka (2004), except Reaction 0. The kinetic
140   rate constant of the solid phase CO₂(g*) dissolution (i.e., soil CO₂ production rate constant) was from (Bengtson and Bengtsson, 2007;Ahrens et al., 2015;Carey et al., 2016); The specific surface area was referred to that of soil organic carbon (Pennell et al., 1995).
e. These reactions were only used in the base case model as they occurred in shallow soils in Konza. In the later numerical experiments, these reactions were not included so as to focus on carbonate weathering.

145

Table 2. Measured CO₂(g) at different depths and corresponding estimated $C_{CO_2(aq)}$

	Time	Soil depth				Ways obtained[a,b,c]
I.	**Grassland (Konza) cases**					
		Horizon A (h = 16 cm)	Horizon AB (84 cm)	Horizon B (152 cm)	Groundwater (366 cm)	
Soil T °C		17	15	13	8	Estimated
K_1		4.1×10^{-2}	4.4×10^{-2}	4.6×10^{-2}	5.4×10^{-2}	Estimated
	1. Base case with monthly updated CO₂(g) (%) and CO₂(aq) (mol/L)					
CO₂(g)	July	3.6	6.8	6.6	2.2	Measured
	August	1.4	1.7	7.2	3.9	Measured
	September	0.6	1.2	3.9	4.9	Measured
	October	0.5	1.4	2.5	5.0	Measured
	November	0.6	1.1	2.2	4.0	Measured
	January	0.3	0.8	1.1	3.6	Measured
	March	0.2	0.3	0.5	3.0	Measured
$CO_2(aq)$	July	1.5×10^{-3}	3.0×10^{-3}	3.0×10^{-3}	1.2×10^{-3}	Estimated
	August	5.7×10^{-4}	7.5×10^{-4}	3.3×10^{-3}	2.1×10^{-3}	Estimated
	September	2.5×10^{-4}	6.2×10^{-4}	1.8×10^{-3}	2.6×10^{-3}	Estimated
	October	1.9×10^{-4}	6.2×10^{-4}	1.2×10^{-3}	2.7×10^{-3}	Estimated
	November	2.5×10^{-4}	4.8×10^{-4}	1.0×10^{-3}	2.2×10^{-3}	Estimated

		January	1.2×10⁻⁴	3.5×10⁻⁴	5.1×10⁻⁴	1.9×10⁻³	Estimated
		March	8.2×10⁻⁵	1.3×10⁻⁴	2.3×10⁻⁴	1.6×10⁻³	Estimated
2.	*Numerical experiments with annual average CO₂(g) (%) and CO₂(aq) (mol/L)*						
$CO_2(g)$		Annual	1.0±1.2	1.9±2.2	3.4±2.6	3.8±1.0	Measured
$\underline{CO_2(aq)}$		Annual	(4.2±5.0)×10⁻⁴	(8.5±9.7)×10⁻⁴	(1.6±1.2)×10⁻³	(2.0±0.5)×10⁻³	Estimated
II.	**Woodland cases (Calhoun, South Carolina)**						
	Numerical experiments with annual average CO₂(g) (%) and CO₂(aq) (mol/L)						
			(h = 50 cm)	(150 cm)	(300 cm)	(500 cm)	
Soil T °C			16	13	10	8	Estimated
K_1			4.2×10⁻²	4.6×10⁻²	4.9×10⁻²	5.4×10⁻²	Estimated
$CO_2(g)$		Annual	0.9±0.1	2.7±0.6	3.8±0.6	3.9±0.7	Measured
$\underline{CO_2(aq)}$		Annual	(4.5±0.7)×10⁻⁴	(1.3±0.3)×10⁻³	(1.9±0.3)×10⁻³	(1.9±0.3)×10⁻³	Estimated

a. Monthly measured soil CO_2 data for the Konza grassland (base case) were from (Tsypin and Macpherson, 2012); The annual-average soil CO_2 used in the grassland experiments was averaged from the corresponding monthly measurements. More information on measurements at the Konza grassland were detailed in the SI. The annual-average soil CO_2 in the woodland experiments was from the Calhoun site in South Carolina where trees (forest) are dominant (Billings et al., 2018).

b. $CO_2(aq)$ were estimated using Henry's law $C_{CO_2(aq)} = K_1 pCO_2$; The temperature-dependent K_1 was calculated following Eq. S1. The $C_{CO_2(aq)}$ values at different soil depths were used to prescribe the available soil CO_2 for chemical weathering.

c. Soil temperature was estimated from the soil water and shallow groundwater temperature (Tsypin and Macpherson, 2012;Billings et al., 2018).

Reactions. The shallow soils have more anorthite ($CaAl_2Si_2O_8(s)$) and K-feldspar ($KAlSi_3O_8(s)$) and deeper subsurface contains more calcite (Table S1). Table 1 summarizes reactions and thermodynamic and kinetic parameters. Soil CO_2 increases pore water acidity (Reactions 0-2) and accelerates mineral dissolution (Reactions 3-6). Silicate dissolution leads to the precipitation of clay (represented by kaolinite in Reaction 7). These reactions were included in the base case to reproduce field data. The kinetics follows the transition state theory (TST) rate law (Plummer et al., 1978) $r = kA\left(1 - \frac{IAP}{K_{eq}}\right)$, where k is the kinetic rate constant (mol/m²/s), A is the mineral surface area per unit volume (m²/m³), IAP is the ion activity product, and K_{eq} is the equilibrium constant. The term IAP/K_{eq} quantifies the extent of disequilibrium: values close to 0 suggest far from equilibrium whereas values close to 1.0 indicate close to equilibrium.

Flow partitioning. Rain water entered soil columns at the annual infiltration rate of 0.37 m/yr, estimated based on the difference between measured precipitation (0.88 m/yr) and evapotranspiration (0.51 m/yr). At 50 cm, a lateral flow Q_L (soil water) exited the soil column to the stream at 0.35 m/yr. The rest recharged the deeper domain beyond 50 cm (to the groundwater system) at 0.02 m/yr (~ 2% of precipitation) and became groundwater (Figure 1A), a conservative value compared to 2-15% reported in another study (Steward et al., 2011). The groundwater flow Q_G eventually came out at 366.0 cm and was assumed to enter the stream as part of discharge (= $Q_L + Q_G$). The flow field was implemented in CrunchTope using the "PUMP" option.

Calibration. We used monthly measured alkalinity and Ca concentration data in different horizons (Horizon A, B and groundwater in Figure 2A) from 2009-2010 at the Konza grassland for model calibration. The monthly Nash-Sutcliffe efficiency (NSE), which quantified the residual variance of modeling output compared to measurements, was used for model performance evaluation (Moriasi et al., 2007). NSE values higher than 0.5 are considered acceptable. At Konza, calcite in the shallow soil (above Horizon B) is mixed with other minerals, has small particle size, and is considered "impure" (Macpherson and Sullivan, 2019) and therefore has a lower K_{eq} value than those at depth with relatively "pure" calcite. The K_{eq} of "impure" calcite (K_4) was calibrated by fitting field data of Ca and alkalinity.

3.2 Numerical experiments

Numerical experiments were set up to understand how and to what extent roots regulate weathering rates and solute
180   transport in grasslands and in woodlands. The base case from Konza was used to represent grasslands, and the Calhoun site (the
Calhoun Critical Zone Observatory in South Carolina, USA) was used as a representative woody site (Billings et al., 2018).
Grasslands are typically characterized by a high proportion of horizontal macropores induced by dense, lateral-spread of roots
mostly at depths less than 0.8 m (Jackson et al., 1996;Frank et al., 2010). These characteristics promote lateral flow (Q_L) at the
shallow subsurface (Figure 1A). At Konza, > 90% of grass roots were at the top 0.5 m, leading to high hydrologic conductivity in
185   top soils (Nippert et al., 2012). In the woodland, a greater proportion of deep roots enhances vertical macropore development
(Canadell et al., 1996;Nardini et al., 2016), reduces permeability contrasts at different depths (Vergani and Graf, 2016), and is
thought to facilitate more vertical water flow to the depth (Q_G). At the Calhoun site, > 50% of roots are in the top 0.5 m in
woodlands, with the rest penetrating deeper (Jackson et al., 1996;Eberbach, 2003;Billings et al., 2018).

The experiments aimed to compare the general, averaged behaviors rather than event-scale dynamics so the annual-
190   average soil CO_2 data and corresponding prescribed CO_2(aq) concentrations were used (Table 2). The experiments focused on
calcite weathering (Reaction 0-4) and excluded silicate weathering reactions (Reaction 5-7). The mineral-dissolution-related
parameters from the base case were used for all experiments. We compared the relative significance of hydrological and
biogeochemical effects (soil CO_2 level and distribution) of rooting depths.

Hydrological and bigeochemical differences in grasslands and woodlands. Flow partitioning between lateral shallow
195   flow and vertical recharge flow is challenging to quantify and is subject to large uncertainties under diverse climate, lithology, and
land cover conditions. The ratios of lateral flow in shallow soils versus the total flow inferred from a tracer study in a grassland
vary from ~70% to ~95% (Weiler and Naef, 2003). Harman and Cosans (2019) found that the lateral flow rate at shallow soils
over the overall infiltration can vary between 50% and 95%. Deeper roots in woodlands can increase deep soil permeability by >
one order of magnitude (Vergani and Graf, 2016). Assuming that the vertical, recharged flow water ultimately leaves the watershed
200   as baseflow, the ratio of the lateral versus vertical flow has been reported with a wide range. In forests such as Shale Hills in
Pennsylvania and Coal Creek in Colorado, ~ 7%-20% of stream discharge is from groundwater, presumably recharged by vertical
flow (Li et al., 2017;Zhi et al., 2019). Values of Q_G/Q_T estimated through base flow separation vary from 20% to 90% in
forest/wood-dominated watersheds (Price, 2011), often negatively correlating with the proportion of grasslands (Mazvimavi et al.,
2004).
205   Soil respiration rates can vary between 10^{-9} ~ 10^{-5} mol/m^2/s for both grasslands and woodlands (Bengtson and Bengtsson,
2007;Ahrens et al., 2015;Carey et al., 2016). Soil CO_2 levels may vary by 2-3 orders of magnitude depending on vegetation type
and climate conditions (Neff and Hooper, 2002;Breecker et al., 2010). Soil CO_2 levels are further complicated also by their
dependence on topographic position, soil depth, and soil moisture, all of which determine the magnitude of microbial and root
activities and CO_2 diffusion (Hasenmueller et al., 2015;Billings et al., 2018). There is however no consistent evidence suggesting
210   which land cover exhibits higher soil respiration rate or soil CO_2 level. Below we describe details of the numerical experiments
(Table 3) exploring the influence of hydrological versus biogeochemical impacts of roots.

215

Table 3. Physical and geochemical characteristics in numerical experiments[a]

	Cases	Calcite distribution[b]	Hydrological and biogeochemical aspects		
			Schematic	Flow partitioning[c]	Soil CO_2 distribution[d]
Scenario 1 with flow partitioning (PF)	Grass$_{PF}$			$Q_L = 95\% \; Q_T$ $Q_G = 5\% \; Q_T$ (red arrow)	Annual average from the Konza grassland (red line)
	Wood$_{PF}$			$Q_L = 60\% \; Q_T$ $Q_G = 40\% \; Q_T$ (blue arrow)	Annual average from the Calhoun forest (blue line)
Scenario 2 with 100% vertical flow (VF)	Grass$_{VF}$			$Q_L = 0$ $Q_G = Q_T$ (black arrow)	Annual average from the Konza grassland (red line)
	Wood$_{VF}$				Annual average from the Calhoun forest (blue line)
Scenario 3 with 100% lateral flow (HF)	Grass$_{HF}$			$Q_L = Q_T$ $Q_G = 0$ (black arrow)	Annual average from the Konza grassland (red line)
	Wood$_{HF}$				Annual average from the Calhoun forest (blue line)

a. Diagrams represent the soil profiles of physical and geochemical properties;
b. Calcite distribution (black line) in all cases increases with depth;
c. The flow field was implemented in CrunchTope using the "PUMP" option;
d. Annual-average soil CO_2 used for constraining the grassland (red line) was from the Konza grassland (Tsypin and Macpherson, 2012). The annual-average soil CO_2 in the woodland (blue line) was from the Calhoun forest (Billings et al., 2018).

Three scenarios. Each scenario in Table 3 includes a grassland and woodland case, with their respective profiles of calcite distribution and soil pCO_2 kept the same (column 3 and 4 in Table 3). The only difference in different scenarios is the flow partitioning (column 5 in Table 3). Soil pCO_2 in the grassland (red line in Table 3) were set to reflect the annual average of the Konza site. Soil pCO_2 (blue line) in the woodland is the annual average from the forest-dominant Calhoun site (Billings et al., 2018). In all scenarios, we assumed that grasslands and woodlands had the same total solid phase "$CO_2(g^*)$" producing CO_2 gas and $CO_2(aq)$ but differed in depth distributions. The $CO_2(g^*)$ served as the source of soil CO_2 and was constrained by $CO_2(g)$ field data (Table 2). In grasslands, the modeled distribution of $CO_2(g^*)$ was steep, with higher density of roots and more abundant $CO_2(g^*)$ in the shallow soils; while the distribution was less steep in woodlands (Jackson et al., 1996). Below the rooting depth, $CO_2(g^*)$ was assumed to be smaller (by 10 times) to represent the potential soil CO_2 sources from microbial activities (Billings et al., 2018).

Scenario 1 considered flow partitioning (Table 3). With the large permeability contrast of soil and bedrock (over four orders of magnitude) in Konza (Macpherson, 1996), the Grass$_{PF}$ case (with $Q_L = 95\% \times Q_T$ and $Q_G = 5\% \times Q_T$) represents an end-member case for the grassland. The woodland (Wood$_{PF}$) case was set to have 60% lateral flow and 40% vertical flow into deeper subsurface. This groundwater percentage is at the high end of flow partitioning and serves as an end-member case for woodlands (Vergani and Graf, 2016). Scenarios 2 and 3 had no flow partitioning. Scenario 2 had two cases with 100% vertical flow via the bottom outlet (VF; Wood$_{VF}$ and Grass$_{VF}$); Scenarios 3 had two cases with 100% horizontal flow (HF; Wood$_{HF}$ and Grass$_{HF}$) via the shallow outlet at 50 cm. These cases represent the end-member flow cases with 100% lateral flow or 100% vertical flow. In addition, because the two cases have the same flow scheme, they enable the differentiation of effects of soil CO_2 distribution versus hydrology differences. All scenarios were run under infiltration rates from 3.7×10^{-2} to 3.7 m/yr ($10^{-4} – 10^{-2}$ m/day), the observed daily variation range at Konza. This was to explore the role of flow regimes and identify conditions where most and least significant differences occur. To reproduce the observed soil CO_2 profile, the soil CO_2 production rate (mol/m^2/yr) at the domain scale (calculated by the mass change of the solid phase $CO_2(g^*)$ over time) was assumed to increase with infiltration rates (Figure S2).

This is consistent with field observations that soil CO_2 production rate and efflux may increase with rainfall in grassland and forest ecosystems (Harper et al., 2005;Patrick et al., 2007;Wu et al., 2011;Vargas et al., 2012;Jiang et al., 2013). For example, Zhou et

250   al. (2009) documented soil CO_2 production rates increasing from 3.2 to 63.0 mol/m^2/yr when the annual precipitation increased from 400 to 1,200 mm. In addition, Wu et al. (2011) showed that increasing precipitation from 5 to 2,148 mm enhanced soil respiration by 40% and that a global increase in 2 mm precipitation per decade may lead to an increase of 3.8 mol/m^2/yr for soil CO_2 production. The simulated soil CO_2 production rates across different infiltration rates here (~0.1-10 mol/m^2/yr shown in Figure S2) were close to the reported belowground net primary production (belowground NPP) of typical ecosystems: ~0.8-100 mol/m^2/yr

255   for grasslands (Gill et al., 2002) and ~ 0.4 - 40 mol/m^2/yr for woodlands (Aragao et al., 2009).

Each case was run until steady state, when concentrations at the domain outlet became constant (within ±5%) over time. The time to reach steady state varied from 0.1 to 30 yrs, depending on infiltration rates. The lateral flux (soil water, $M_L=Q_L \times C_L$) and vertical fluxes (groundwater, $M_G=Q_G \times C_G$) were calculated at 50 and 366 cm, in addition to total fluxes (weathering rates, M_T). These fluxes multiplied with unit cross-section area (m^2) convert into rates in units of mol/yr.

260   *Carbonate weathering over century time scales: soil property evolution.* To compare the propagation of weathering fronts over longer time scales, we carried out two 300-yr simulations for Scenario 1 with flow partitioning under the base-case infiltration rate of 0.37 m/yr (i.e., Grass$_{PF}$ and Wood$_{PF}$ in Table 3). During this long-term simulation, we updated calcite volume, porosity and permeability. The calcite volume changes were updated in each time step based on corresponding mass changes, which were used to update porosity. Permeability changes were updated based on changes in local porosity following the Kozeny-Carman equation:

265    $\frac{k_i}{k_{i,0}} = \left(\frac{\emptyset_i}{\emptyset_{i,0}}\right)^3 \times \left(\frac{1-\emptyset_{i,0}}{1-\emptyset_i}\right)^2$ (Kozeny, 1927;Costa, 2006), where k_i and $\emptyset_i$ is permeability and porosity in grid i at time t, and $k_{i,0}$ and $\emptyset_{i,0}$ are the initial permeability and porosity, respectively.

3.3 Quantification of weathering rates and their dependence on CO_2-carbonate contact

To quantify the overall weathering rates and CO_2-carbonate contact in each scenario, we used the framework from a previously-developed upscaled rate law for dissolution of spatially heterogeneously distributed minerals (Wen and Li, 2018). The

270   rate law says that three characteristics times are important. The equilibrium time τ_{eq} represents the characteristic timescale of mineral dissolution to reach equilibrium in a well-mixed system. The residence time τ_a, i.e., the timescale of advection, quantifies the overall water contact time with the whole domain. It was calculated by the product of domain length (L) and porosity divided by the overall infiltration rate (Q_T): $\tau_a = \frac{L\phi}{Q_T}$. The reactive transport time $\tau_{ad,r}$ quantified the water contact time with calcite as influenced by both advection and diffusion/dispersion. The upscaled rate law is as follows:

275    $$R_{calcite} = k_{calcite}A_T\left[1 - exp\left(-\frac{\tau_{eq}}{\tau_a}\right)\right]\left\{1 - exp\left[-L\left(\frac{\tau_a}{\tau_{ad,r}}\right)\right]\right\}^\alpha \qquad (1)$$

Here k is the intrinsic rate constant measured for a mineral in a well-mixed reactor, A_T is the total surface area, L is domain length, α is geostatistical characteristics of spatial heterogeneity, and $\frac{\tau_a}{\tau_{ad,r}}$ is the reactive time ratio quantifying the relative magnitude of the water contact time with the whole domain versus the contact time with the reacting mineral. This rate law consists of two parts: the effective dissolution rates in homogeneous media represented by $kA_T\left[1 - exp\left(-\frac{\tau_{eq}}{\tau_a}\right)\right]$ and the heterogeneity factor

280    $\left\{1 - exp\left[-L\left(\frac{\tau_a}{\tau_{ad,r}}\right)\right]\right\}^\alpha$ that quantifies effects of preferential flow paths arising from heterogeneous distribution of minerals. When

$\frac{\tau_a}{\tau_{ad,r}} > 1$, the water contact time with calcite zone is small, meaning the water is replenished quickly compared to the whole domain, leading to higher CO_2-carbonate interactions. In contrast, small $\frac{\tau_a}{\tau_{ad,r}}$ ratio (<1) reflects water is replenished slowly in the reactive calcite zones, leading to less CO_2-carbonte contact. These different time scales were calculated for Scenarios 1-3 based on the flow characteristics and dissolution thermodynamics and kinetics, as detailed in the SI. Values of τ_{eq}, τ_a, and $\tau_{ad,r}$ for all experiments

285   are listed in Table S2.

4 Results

4.1 The thermodynamics of carbonate dissolution: grassland at Konza as the base case scenario

The calibrated model reproduced the temporal dynamics with a Nash-Sutcliffe efficiency (NSE) value > 0.6 and was considered satisfactory (Figure 2). Note that y axis is inverted to display shallow soils at the top and deep soils at the bottom to be

290   consistent with their subsurface position shown in Figure 2A. The measured $CO_2(g)$ varied between 0.24 – 7.30% (Figure 2B right axis), one to two orders of magnitude higher than the atmospheric level of 0.04%. The estimated $CO_2(aq)$ (Figure 2B left axis) generally increased with depth except in July and August when horizon B was at peak concentration. The timing of the peaks and valleys varied in different horizons. The $CO_2(aq)$ reached maxima in summer in soil horizons A and B and decreased to < 0.5 mM in winter and spring. The groundwater $CO_2(aq)$ exhibited a delayed peak in September and October, and dampened seasonal

295   variation compared to soil horizons. The temporal trends of alkalinity, DIC, and Ca in groundwater mirrored those of soil CO_2 at their corresponding depths, indicating the predominate control of soil CO_2 on carbonate weathering. The groundwater concentrations of these species were also higher than soil concentrations. The simulated groundwater DIC (approximately summation of $CO_2(aq)$ and alkalinity) was > 6 times higher than that in shallow soil (~ 1.0 mM). The dissolved mineral volume was negligible for the simulation period (< 0.5% v/v). Sensitivity analysis revealed that changes in flow velocities influenced

300   concentrations in Horizon A with anorthite as the dominating dissolving mineral (0 – 1.8 m); their effects are negligible in Horizon B and groundwater where fast-dissolving calcite has reached equilibrium.
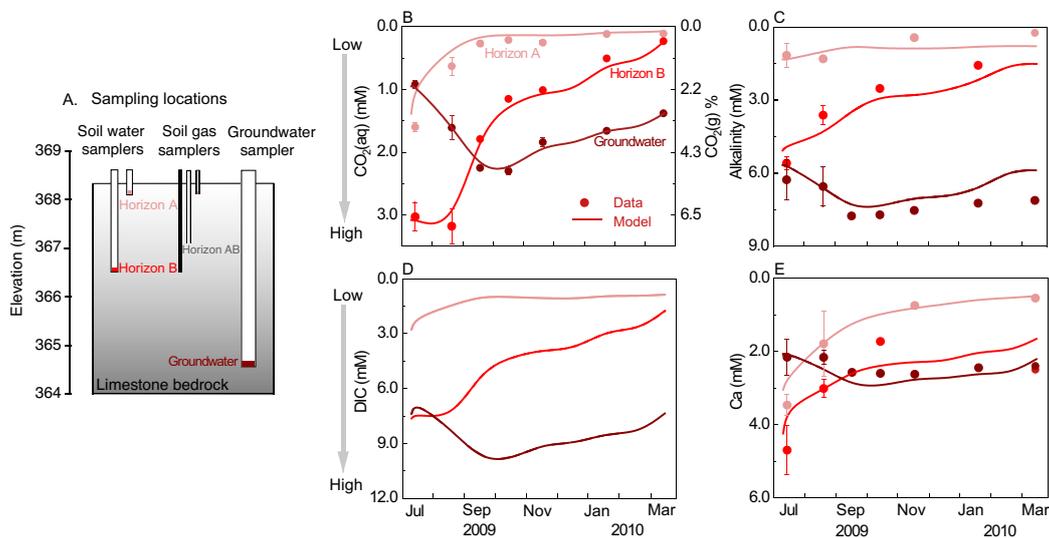
Figure 2. (A) Schematic representation of sampling depths in the Konza grassland; Corresponding monthly dynamics of (B) $CO_2(aq)$ and $CO_2(g)$, (C) alkalinity, (D) DIC, and (E) Ca concentrations. Lines represent modelling outputs at the

305   corresponding sampling depth of monthly field measurements (dots), including soil water at Horizons A (16 cm) and B (152 cm), and groundwater (366 cm). The lines of $CO_2(aq)$ and $CO_2(g)$ in Figure B overlapped. Note that there are no DIC data so no dots in Figure D. The temporal trends of alkalinity, DIC, and Ca mirrored those of soil CO_2, indicating its predominant control on weathering.

    Several measurements/parameters were important in reproducing data, especially soil CO_2 that determined the $CO_2(aq)$

310   level and its spatial variation, and equilibrium constant (K_{eq}) of calcite dissolution. Imposition of monthly variations and depth distributions of soil CO_2 were essential to capture the variation of alkalinity and Ca data at different horizons. The imposition of calcite K_{eq} was also critical for reproducing Ca concentrations. Impurities were suggested to affect K_{eq} of natural calcite by a factor of ~2.0 (Macpherson and Sullivan, 2019). Calcite K_{eq} in shallow soils had to be reduced by a factor of 3.8 in the model to reproduce concentrations in Horizon A. The alkalinity and Ca concentrations were not sensitive to kinetic parameters nor precipitation,

315   because carbonate dissolution was fast and thermodynamically controlled.

4.2 Numerical experiments: the significance of potential hydrology differences

    Scenario 1 for hydro-biogeochemical effects with flow partitioning (Wood_PF and Grass_PF). Figures 3A1-E1 show depth profiles of calcite and soil CO_2 production rates and steady-state concentrations of reaction products. Although the model did not explicitly simulate soil respiration, the soil CO_2 production rate was highest in the shallow soil at around $10^{-6.5}$ mol/s and

320   decreased to ~ $10^{-9.5}$ mol/s at 366 cm (Figure 3B1), consistent with the decline with soil depth observed in natural systems. The $CO_2(g)$ level (released from the solid phase $CO_2(g^*)$) increased with depth due to autotrophic and heterotrophic respiration and downward fluxes of CO_2-charge water from the shallow soil (Figure 3C1). Concentrations of reaction products (Ca, DIC) were lower in the top 40 cm reflecting the lower carbonate-mineral background level and higher at depths > 60 cm. The transition occurred between 35 cm – 60 cm at the vicinity of calcite-no calcite interface at 55 cm, where concentrations of Ca and DIC

325   increased abruptly until reaching equilibrium. This thin transition was driven by fast calcite dissolution and rapid approach to equilibrium, resulting in a short equilibrium distance. The equilibrated DIC and Ca concentrations below 60 cm followed the similar increasing trend of $CO_2(g)$ with depth in the deep zone (Figure 3C1-E1).

    Figures 3F1 show that Ca concentrations in soil water (light color) were lower than groundwater (dark color) and varied with infiltration rates. The difference between soil water and groundwater Ca concentrations was relatively small at low infiltration

330   rates because both reached equilibrium but diverged at high infiltration rates. Higher infiltration rates diluted soil water but not as much for groundwater. As expected, stream concentrations, a mixture of soil water and groundwater (solid line), were in between these values but closely resembled soil water in the grassland. In both cases, stream concentration decreased as infiltration increased, indicating a dilution concentration-discharge relationship.
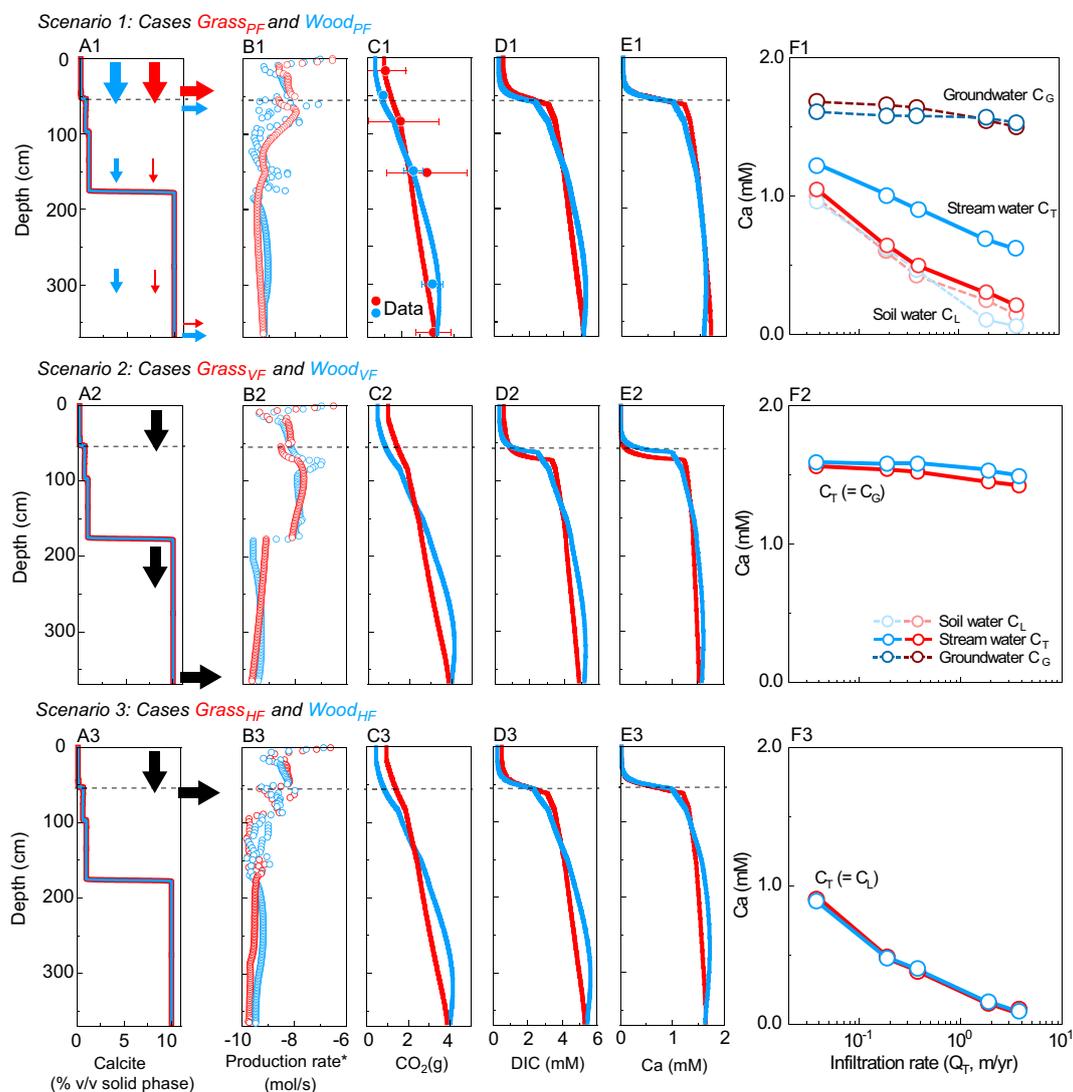
Figure 3. Simulated depth profiles of (A) calcite (vol %), (B) soil CO_2 production rate; (C) $CO_2(g)$, (D) DIC, and (E) Ca at 0.37 m/yr, and (F) effluent Ca concentrations at different infiltration rates. From top to bottom rows are Scenario 1 ($Grass_{PF}$ and $Wood_{PF}$; with flow partitioning, first row), Scenario 2 ($Grass_{VF}$ and $Wood_{VF}$; 100% vertical flow, second row), and Scenario 3 ($Grass_{HF}$ and $Wood_{HF}$; 100% lateral flow, last row). Red and blue colors present grassland and woodland, respectively. Lines and empty circles represent modelling outputs while filled circles with error bar in Figure C are the annual average $CO_2(g)$ data (in Table 2). Arrows in Figure A indicate flow conditions. In F, soil water and groundwater refer to concentrations at the lateral (50 cm) and vertical (366 cm) outlets, respectively. Higher fractions of vertical flow in $Wood_{PF}$ led to higher stream Ca concentration compared to $Grass_{PF}$. In Scenarios 2 and 3 without flow partitioning, stream Ca concentrations were similar. The concentrations of DIC versus discharge are very similar to the Ca concentrations in F.

Scenarios 2-3 for biogeochemical effects (without flow partitioning). Scenarios 2 and 3 were end-member cases that bracket the range of rooting effects. Calcite and soil CO_2 were distributed the same way as their corresponding PF cases (Table 3). The $Wood_{VF}$ and $Grass_{VF}$ cases had 100% flow going downward via the deeper calcite zone maximizing the CO_2-water-calcite contact.

In the Wood_HF and Grass_HF cases (Table 3), all water exited at 50 cm, bypassing the deeper calcite-abundant zone, minimizing the
350 CO_2-water-calcite contact. Figures 3A2-F2 and 3A3-F3 show the VF (Wood_VF and Grass_VF) and HF (Wood_HF and Grass_HF) cases,
respectively. Similar to the flow partitioning cases, the concentrations of reaction products were low in the shallow zone and
increased over 10 times within a short distance ~ 5 cm at the depth of ~ 50 cm. The woodland cases increased slightly more than
the grassland cases because of the slightly steeper soil CO_2 distribution (Figure 3C2 and 3C3). Figure 3F2 indicates that the effluent
Ca concentrations were slightly higher in Wood_VF due to the high soil CO_2 level at the bottom outlet. The Grass_HF and Wood_HF
355 case almost had the same effluent Ca concentrations, at the shallow soil (Figure 3F3).

Concentration-discharge relationship and weathering rates in all cases. The VF cases had the highest effluent concentrations
and weathering rates, whereas the HF cases had lowest concentrations and weathering rates, and the Grass_PF and Wood_PF cases fell
in between (Figure 4A-B). This is because the VF cases maximized the CO_2-calcite contact with 100% flow through the calcite
zone, whereas the HF cases had minimum CO_2-calcite contact with water bypassing the calcite zone (column 3-4 in Table 3). The
360 Grass_PF and Wood_PF cases allowed different extent of contact prescribed by the amount of flow via the calcite zone. A case run
without soil respiration (i.e., no $CO_2(g^*)$, not shown) indicated that Ca and DIC concentrations were more than an order of
magnitude lower than cases with soil respiration. In addition, the PF and HF cases generally showed dilution patterns with
concentration decreasing with infiltration rates, as compared to the VF cases where a chemostatic pattern emerge with almost no
changes with infiltration rates. This is because in the VF cases, the concentrations mostly reached equilibrium concentration. In
365 PF and HF cases, a large proportion of water flow through soils with negligible calcite where the water becomes further away from
equilibrium as infiltration rates increase.
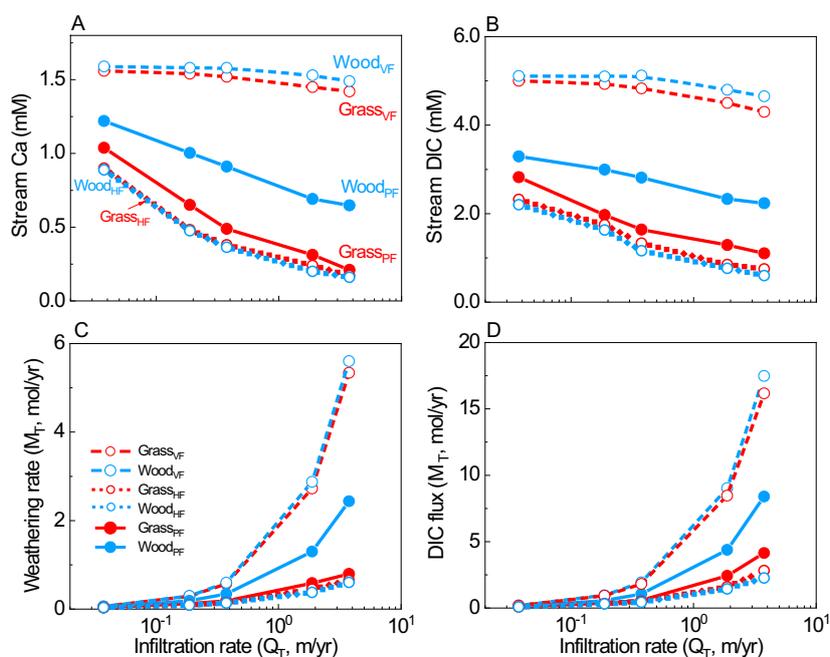
Figure 4. (A-B) Stream water Ca and DIC concentrations, and (C-D) stream fluxes from all scenarios. Stream water
was the overall effluent from soil water and groundwater. The differences caused by hydrological differences (VF, HF,
370 and PF) were much larger than the differences within each pair with the same flow partitioning, indicating significant
hydrological impacts on weathering. The Ca fluxes in the VF cases (100% vertical flow) were higher than flow
partitioning cases because they enabled maximum CO_2-charged water content with unweathered calcite at depth.

Within each pair with the same flow pattern, the difference was mainly due to the distribution of soil CO_2. The difference

375 of weathering fluxes was 1-12% and 1-5% between HF cases and VF cases, respectively, much smaller than differences between the PF cases. Comparing the HF and VF cases, differences in weathering fluxes was 73% at 3.7×10^{-2} m/yr and 721% at 3.7 m/yr, about 1-2 orders of magnitude higher than differences induced by soil CO_2 distribution. Between the $Grass_{PF}$ and $Wood_{PF}$ cases, the differences were in the range of 17%-207% at the flow range of 3.7×10^{-2} - 3.7 m/yr. The DIC fluxes showed similar trends (Figure 4D).

380 Although weathering rates generally increased with infiltration rates, the woodland increased more (4.6×10^{-2} to 2.4 mol/yr in $Wood_{PF}$). Estimates of the overall soil CO_2 production rate in $Grass_{PF}$ and $Wood_{PF}$ suggest that the values under the same infiltration rate were all within a difference of 10% (Figure S2), indicating that the difference of weathering rates are mainly driven by the flow partitioning. As a reference, the weathering rate in cases with soil respiration was up to 10 times higher compared to that without soil respiration.

385 **Development of reaction fronts at the century scale.** To explore the longer-term effects, we ran the PF cases at 0.37 m/yr for 300 years. More water flowing vertically through abundant calcite zones in $Wood_{PF}$ resulted in faster weathering and deeper reaction front at a depth of ~210 cm compared to ~95 cm in $Grass_{PF}$ (Figure 5A). The depletion of calcite led to an increase of porosity (Figure 5B), which was over one order of magnitude higher at the domain scale of the woodland than that in the grassland (Figure 5C). Permeability evolution had the similar trend with porosity (not shown here). This indicates that if deeper roots promoted more water into deeper soils, they would push reaction fronts deeper and controlled the position where chemically

390 unweathered bedrock was transformed into weathered bedrock. At time scales longer than century scale, calcite may become depleted, which ultimately reduces weathering rates (White and Brantley, 2003) and lead to similar weathering fronts in grasslands and woodlands.
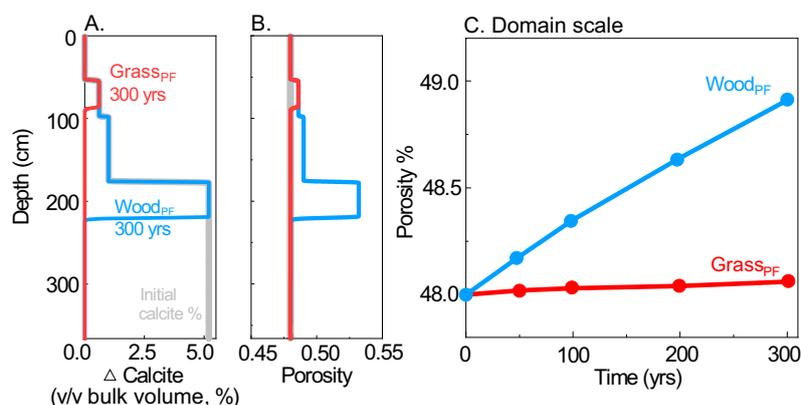
395 Figure 5. Predicted soil profiles of (A) calcite volume change (△Calcite = initial calcite volume - current calcite volume) and (B) porosity after 300 years; (C) Predicted temporal evolution of domain-scale porosity in the grassland and woodland. The infiltration rate is 0.37 m/yr. Red and blue line represents the case $Grass_{PF}$ and $Wood_{PF}$, respectively.

4.3 The regulation of weathering rates by CO_2-carbonate contact

Natural systems are characterized by preferential flow paths such that flow distribution is not uniform in space.

400 Weathering in such systems with preferential flow in zones of differing reactivities have been shown to hinge on the contact time

between water and the reacting minerals instead of all minerals that are present (Wen and Li, 2018) (Eq. 1). Here we contextualize the weathering rates in different scenarios (symbols) with predictions from an upscaled rate law developed by Wen and Li (2018) that incorporate the effects of heterogeneities in flow paths (Figure 6). The time ratio $\frac{\tau_a}{\tau_{ad,r}}$ compares the domain water contact time (or residence time) with the contact time with dissolving calcite. In Grass$_{VF}$ and Wood$_{VF}$ (open circles) where all CO_2-charged

405   water flew through the deeper calcite zones, CO_2-calcite interactions reached maximum such that values of $\frac{\tau_a}{\tau_{ad,r}}$ approached 1.0, meaning all water interacted with calcite. Under this condition, weathering rates are the highest among all cases. In contrast, in Wood$_{HF}$ and Grass$_{HF}$ (open diamonds) where all CO_2-charged water bypassed the deeper calcite zone, $\frac{\tau_a}{\tau_{ad,r}}$ can be 1-3 orders of magnitude lower and weathering rates were at their minima. The $\frac{\tau_a}{\tau_{ad,r}}$ value in the water partitioning cases (Grass$_{PF}$ and Wood$_{PF}$, filled circles) fell in between. At the same τ_a, the Wood$_{PF}$ case with deepening roots promoted CO_2-water-calcite contact (i.e.,

410   larger $\frac{\tau_a}{\tau_{ad,r}}$), and dissolved calcite at higher rates.

The magnitude of rate difference also depends on the overall flow rates (or domain contact time τ_a). At fast flow with small τ_a (large symbols and thick lines in Figure 6), flow partitioning has a larger influence. At τ_a of 0.47 year, the weathering rates in the VF cases were more than an order of magnitude higher than those in the PF cases. The weathering rate in the woodland was over 7 times that of the grassland. In contrast, at τ_a of 47 years, the rate differences between grass- and woody- cases were less

415   than 25%, largely because the dissolution has reached equilibrium. In the VF and HF cases where flow conditions were the same, the soil CO_2 distribution in grassland and woodland differed only slightly, leading to similar values of $\frac{\tau_a}{\tau_{ad,r}}$ and weathering rates and indicating minimal impacts of soil CO_2 distribution. These rates from numerical experiments closely follow the prediction from the upscaled reaction rate law (grey lines, Eq. 1). The rate law predicted that weathering rates increased from HF cases with small $\frac{\tau_a}{\tau_{ad,r}}$ values to VF cases where $\frac{\tau_a}{\tau_{ad,r}}$ approached 1. It also showed that weathering rates reached their maxima in homogeneous

420   domains without flow partitioning.
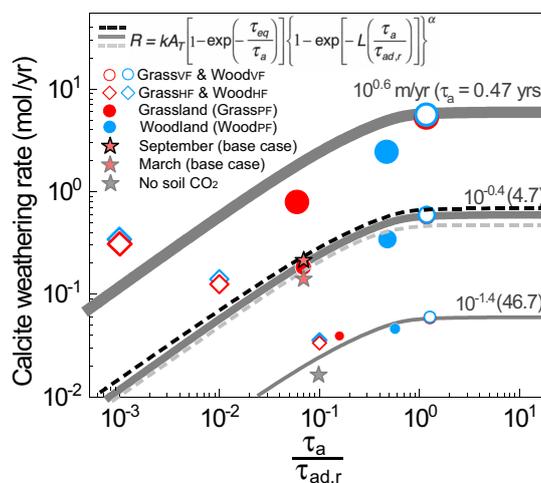
Figure 6. Calcite weathering rate as a function of the reactive time ratio $\frac{\tau_a}{\tau_{ad,r}}$. Symbols are rates from numerical experiments. Grey lines are predictions from the rate law equation at $\alpha = 0.8$ (Wen and Li, 2018). Large to small dots and thick to thin lines are for infiltration rates from $10^{0.6}$ to $10^{-1.4}$ m/yr. The red filled stars represent the monthly rates in

425   September (highest soil CO_2) and March (lowest soil CO_2) in the base case at $10^{-0.4}$ (0.37) m/yr; the black to grey dash lines represent predictions with increasing soil CO_2 level (i.e., larger τ_{eq}) from Eq. (1). Grey filled star is for the case

without soil CO_2. At any specific infiltration rate or τ_a, the VF and HF cases bracket the two ends whereas the PF cases fall in between. The Wood$_{PF}$ case with deeper roots enhanced the CO_2-water-calcite contact (i.e., larger $\frac{\tau_a}{\tau_{ad,r}}$ ratios), leading to higher calcite weathering rates compared to grasslands. The differences of weathering rates induced by
430   different soil CO_2 level were relatively small compared to those hydrological changes induced by rooting depth.

5 Discussion

Because carbonate dissolution is thermodynamically controlled and transport limited, the overall weathering rates depend on how much CO_2-charged water flushes through the carbonate zone. This work indicates that the roots potentially enhance weathering rates in two ways. First, roots can control thermodynamic limits of carbonate dissolution by regulating how much CO_2
435   is transported downward and enters the carbonate-rich zone. In fact, the base-case grassland data and model reveal that the concentrations of Ca and DIC are regulated by seasonal fluctuation of pCO_2 and soil respiration. Second, roots control how much and how frequently water fluxes through the carbonate zone, exports reaction products at equilibrium such that more dissolution can occur. The numerical experiments indicate that carbonate weathering at depth hinges on the rate of delivery of CO_2-enriched water. Deepening roots in woodlands that channel more water into the unweathered carbonate can elevate weathering rates by
440   more than an order of magnitude compared to grasslands. Below we elaborate and discuss these two messages.

5.1 The thermodynamics of carbonate weathering: control of temperature and pCO_2

The base case data and simulation showed that calcite dissolution reaches equilibrium rapidly and is thermodynamically controlled (Section 4.1), which echoes observations from other weathering studies (Tsypin and Macpherson, 2012;Gaillardet et al., 2019). The extent of dissolution, or solubility indicated in Ca and DIC concentrations, is determined by soil CO_2 levels that are
445   a function of ecosystem functioning and climate. In hot, dry summer, soil respiration reaches its maximum rates in shallow soil horizons and pCO_2 peaks (Figure 2). In wet and cold winter, soil pCO_2 plummets, leading to much lower Ca and DIC concentrations. Based on Reactions 0-4 (Table 1) and temperature dependence of equilibrium constants, the following equations can be derived (detailed derivation in the SI) for Ca and DIC concentrations in carbonate-dominated landscapes:

$$C_{Ca} = \sqrt[3]{K_{t,25} exp\left(-\frac{\Delta H_t^\circ}{4R} * \left(\frac{1}{T} - \frac{1}{273.15+25}\right)\right) \cdot pCO_2} \tag{2}$$

450
$$C_{DIC} = 2\sqrt[3]{K_{t,25} exp\left(-\frac{\Delta H_t^\circ}{4R} * \left(\frac{1}{T} - \frac{1}{273.15+25}\right)\right) \cdot pCO_2} + K_{1,25} exp\left(-\frac{\Delta H_1^\circ}{4R} * \left(\frac{1}{T} - \frac{1}{273.15+25}\right)\right) \cdot pCO_2 \tag{3}$$

Here $K_{t,25}$ is the total equilibrium constant K_t $(= \frac{a_{Ca^{2+}} a_{HCO_3^-}^2}{pCO_2} = K_1 K_4)$ of the combined reactions 1 and 4 at 25°C; ΔH_t° is the corresponding standard enthalpy (-35.83 kJ/mol); $K_{1,25}$ and ΔH_1° are the equilibrium constant and standard enthalpy of Reaction 1 (in Table 1); R is the gas constant (=8.314×10^{-3} kJ/K/mol). Eq. 2 and 3 imply that DIC and Ca in shallow soil water (0.2 m) are lower compared to groundwater (3.6 m) in the base case at Konza, due to lower dissolved $CO_2(aq)$ arising from higher temperature
455   and higher diffusion rates in shallow soil.

Eq. 2 and 3 were tested with compiled soil $pCO2$ and spring water chemistry data from 8 carbonate-dominated catchments (Dandurand et al., 1982;Lopez-Chicano et al., 2001;Moral et al., 2008;Ozkul et al., 2010;Kanduc et al., 2012;Calmels et al., 2014;Abongwa and Atekwana, 2015;Huang et al., 2015) (also see the SI for details). Plotting spring-water chemistry against pCO_2 indicates that spring water (as representing groundwater) DIC and Ca concentrations increase with pCO_2 (Figure 7), and Eq. 2-3

460   can describe these data and also DIC and Ca levels from numerical simulations from this work (empty dots in Figure 7). The lines

of Eq. 2-3 describe the relationship at 10 $^{\circ}$C, the mean annual temperature, confirming the thermodynamics-control of carbonate

dissolution by soil CO_2 levels. The equation lines closely predicted Ca and DIC under high pCO_2 and lower pH conditions (< 8.0),

because these conditions ensure the validity of the assumption of negligible CO_3^{2-} in the derivation. The presence of cations and

anions other than Ca and DIC can complicate the solution and can bring significant variations of DIC and Ca concentrations under

465   the same pCO_2 conditions.
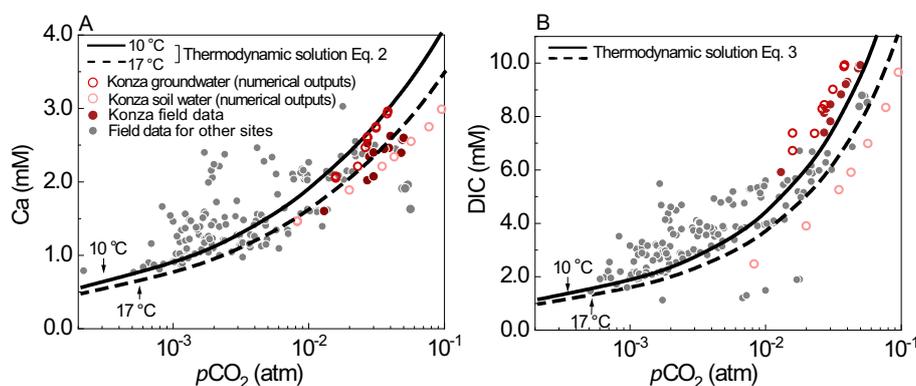
Figure 7. (A) Ca and (B) DIC concentrations from field data in literature (gray dots) and prediction lines. Measured spring water chemistry are from calcite-dominant catchments in literature: Abongwa and Atekwana (2015); Lopez-Chicano et al. (2001); Moral et al. (2008); Huang et al. (2015); Ozkul et al. (2010); Dandurand et al. (1982); Calmels et
470   al. (2014); Kanduc et al. (2012); and Tsypin and Macpherson (2012). Lines are predictions from the thermodynamic solutions (Eq. 2-3) at 10 (solid line) and 17 °C (dash line).

High temperature (T = 17°C) leads to lower DIC and Ca concentrations by about 10% due to the lower calcite and CO_2

solubility at higher T. Higher T also elevates pCO_2 due to higher soil respiration. Various equations exist for predicting soil pCO_2

475   based on climate and ecosystem functioning indicators such as Net Primary Production (NPP) (Cerling, 1984;Goddéris et al.,

2010;Romero-Mujalli et al., 2019a). These equations can be used together with Eq. 2-3 for the estimation of Ca and DIC

concentrations in carbonate-derived waters. Gaillardet et al. (2019) shows that pCO_2 can increase by 2 times with T increase from

9°C to 17°C, which can elevate DIC and Ca concentrations over 50%. Macpherson et al. (2008) observed a 20% increase in

groundwater pCO_2 in Konza over a 15-year period and suggested that increased soil respiration due to climate warming may have

480   elevated soil and groundwater pCO_2. Hasenmueller et al. (2015) demonstrated topographic controls on soil CO_2. Variations of soil

CO_2 and Ca and DIC concentrations therefore are an integrated outcome of climate, soil respiration, subsurface structures, and

hydrological conditions.

5.2 Hydrological controls of root-enhanced carbonate weathering

Evidence from field data. Data in Konza show that although soil pCO_2 peaks in summer, these peaks do not occur right away in

485   deeper groundwater until about 2 months later. Macpherson et al. (2008) and Tsypin and Macpherson (2012) contributed the delay

to the water travel time from soil to groundwater aquifer. The calculation of travel time based on depth difference in soil and

groundwater sampling location (214 cm) and average velocity (0.37 m/year) indicate that it will takes 7-8 months for water to

reach deeper groundwater. The 2 months delay, much shorter than the estimated 7-8 months, suggests that CO_2-charged water may

arrive deeper zones via preferential flow facilitated by roots or via large storm events with much faster flow.

490   The numerical experiments suggest that the root-relevant hydrology can play an essential role in enhancing chemical weathering (Figure 4 and 6). The enhanced weathering rates aligns with observations at Konza that woody-encroached watersheds exhibit higher Ca fluxes in stream and supports the hypothesis that deeper roots can enhance mineral-water interaction via deeper flow paths (Sullivan et al., 2019). Deepening roots can also enhance connectivity between shallow and deeper zones, therefore reducing concentration contrasts between soil water and groundwater. This can lead to more chemostatic C-Q relationships as

495   shown in Wood$_{PF}$ ($b = -0.14$ in $C=aQ^b$) compared to Grass$_{PF}$ ($b = -0.33$) (Figure 4). These findings echo conclusions from Zhi et al. (2019) that chemistry differences in shallow water versus groundwater regulate C-Q patterns. The b values from the C-Q relationships coming out of the 1D modeling (Figure 4) suggest that if flow partitioning is the only difference between the grassland and woody watersheds, a C-Q relationship exhibiting dilution with negative b values is expected in the grassland. The Konza stream data in Sullivan et al. (2019) however showed that C-Q slopes in grasslands ($b = -0.003$) and in woody-encroached lands

500   ($b = 0.013$) are both close to zero (Figure 7 and 8 in Sullivan et al. (2019)). The root influence on C-Q relationship therefore remains equivocal.

Limitations of the model. This discrepancy may suggest that other catchment features that are not represented in the simple 1D model can influence C-Q relationships. The model does not explicitly simulate how and to what degree root distribution at depth alters flow pathways. Instead we focus on the first-order principles of hydrological ramification of roots. The numerical

505   experiments took general observations of rooting characteristics in grasslands and woodlands, and assumed that deepening roots in woodlands promote higher flow partitioning into deep subsurface (Canadell et al., 1996;Nardini et al., 2016;Pawlik et al., 2016). In natural systems, however, other factors can also influence flow partitioning. This includes, for example, contrasts in flow-conducting property (i.e., porosity and permeability) in shallow and deep zones, physical and chemical heterogeneity in carbonate distribution (Wen and Li, 2018), and connectivity between different areas of the catchment in dry and wet times (Wen et al., 2020).

510   Representing these dynamics require a large number of processes and parameters that we do not have data to constrain at this point.

The need for root-relevant measurements. The data-model discrepancy highlights the limitation of a simple model but also points to the need for measurements. In fact, because carbonate weathering is transport-limited and depends largely on water flow via carbonate-rich zones, co-located measurements of rooting characteristics, flow, and water chemistry at depth are essential. Root measurements however rarely go deeper than 30 cm (Richter and Billings, 2015). Existing work exploring root influence on

515   weathering focused primarily on effects of soil CO_2 and root exudates (Drever, 1994;Lawrence et al., 2014;Gaillardet et al., 2019). Although it is well known that roots play a paramount role in modulating macropores and subsurface flow (Fan et al., 2017), the interactions between root characteristics, flow partitioning, and chemical weathering has remained poorly understood. Rooting characteristics depend on climate, plant species, topography, soil properties and geology (Canadell et al., 1996;Mazvimavi et al., 2004;Price, 2011;Nardini et al., 2016). Further studies are needed to characterize root distribution beyond 30 cm, how they vary

520   with intrinsic plant species and external conditions, and how and to what extent they alter subsurface flow. The first step could link rooting characteristics, including density and depth, to soil properties and borrow insights from existing relationships between soil properties and subsurface structure. For example, images of roots and pore structures can be used to characterize the spatiotemporal heterogeneity of fluxes (Renard and Allard, 2013). Geostatistical indices such as permeability variance and correlation length can be used to quantify rooting structure, and relate them to flow partitioning and mineral weathering via numerical experiments (Wen

525   and Li, 2017). The combination of numerical reactive transport experiments built on realistic rooting structure can help develop quantitative relationship between roots and flow partitioning, and could support models for estimating the influence of rooting dynamics on water and carbon cycles at the catchment scale.

5.3 Deepening roots enhance carbon fluxes into deep subsurface: a potential carbon sink?

Mounting evidence has shown that the terrestrial system has become a stronger carbon sink in recent decades (Heimann
530   and Reichstein, 2008), potentially counting for the missing carbon sink as large as ~1 Pg C yr^{-1} in the global carbon budget
(Houghton, 2007;Cole et al., 2007). Although still much debated, recent studies have contributed the downward transport of soil-
respired CO_2 and DIC into groundwater aquifers in deserts as a possible carbon sink in the global carbon cycle (Ma et al., 2014;Li
et al., 2015). Considering the long residence time of DIC in groundwater (10^2-10^4 years) than in the atmosphere (~10^1-10^2 years;
(Archer and Brovkin, 2008)), groundwater may act as a CO_2 storage sink. This work indicated that deepening roots can potentially
535   reroute DIC fluxes to deeper groundwater storage. In particular, vegetation in dry places like deserts often have deep roots (Gupta
et al., 2020). In fact, plants are known for growing deeper roots to tap groundwater during droughts (Brunner et al., 2015).
Deepening roots can enhance downward water drainage (i.e., high vertical connectivity) to the depth and potentially facilitate the
transport of DIC fluxes into deep subsurface. As the pace of climate change accelerates, summer droughts are expected to intensify,
which can potentially channel more CO_2 into the deeper subsurface via deepening roots.

540   With constraints from soil CO_2 data, the simulated CO_2 production rates in Grass$_{PF}$ and Wood$_{PF}$ are similarly at ~ 0.6 mol
C/m^2/yr under the infiltration rate of 0.37 m/yr (Figure S2). This is at the low end of the belowground net production (NPP)
estimations at the Konza site (~2.0-30.0 mol C/m^2/yr) assuming that belowground NPP accounts for 50% of the total NPP (Lett et
al., 2004;Knapp and Ojima, 2014). The simulations showed that in woodlands, the DIC downward fluxes can be > 2.0 times higher
than those in grasslands (Figure 4). In other words, more soil-respired CO_2 can transport to groundwater and become stored there
545   for centuries to millennium before entering a stream. At the short time scale, this enhanced downward transport will reduce CO_2
escape back into the atmosphere. This may explain the observations at Konza that woody encroachment increased NPP however
soil CO_2 flux was significantly reduced compared to the open grassland (Lett et al., 2004). Changing land cover (e.g., woody
encroachment and boreal forest creep) however is not the only mechanism for carbon sink (Stevens et al., 2017;Wang et al., 2020).
Older aged forests also tend to have deepening roots and may act as the carbon sink (Luyssaert et al., 2008), although this is not
550   the case in Konza.

6 Conclusions

This work aims to understand thermodynamic and hydrological control of carbonate weathering driven by deepening
roots. Field data and reactive transport simulation for a grassland in the Konza Prairie LTER site suggest that carbonate dissolution
is thermodynamically controlled and seasonal changes in temperature and pCO$_2$ drives variations of Ca and DIC concentrations in
555   soil water and groundwater. We derived equations based on reaction thermodynamics (Eq. 2-3) to estimate Ca and DIC as a
function of pCO$_2$ and temperature, which has been shown to be applicable in other carbonate-dominated systems. The numerical
experiments probed the potential effects of deepening roots on weathering by channeling a higher proportion of vertically
downward flow (40% of the total) into deep subsurface with abundant calcite. The results show that deeper penetration of roots
and higher recharge flow enhanced CO_2-carbonate contact. At an infiltration rate of 3.7 m/yr, calcite weathering flux in woodlands
560   was 207% higher than that in grasslands. At 3.7×10^{-2} m/yr, the weathering flux in woodland was 17% higher. The hydrological
impacts on carbonate weathering were more than 10 times higher than the biogeochemical impacts via elevated soil CO_2 alone.
The modeling demonstrates that the weathering rates depend on flow partitioning and relative magnitude of water contact time in
the deep carbonate zone. At the century scale, with the assumed higher proportion of vertical flow, the deeper roots pushed the
weathering fronts 2-times deeper, and resulted in a 10-times greater increase in porosity and permeability. Broadly, this deeper
565   propagation of reaction fronts may accelerate rates of channel incision and hillslope erosion (Lebedeva and Brantley, 2013;Brantley
et al., 2017b), and therefore speed up landscape evolution (Phillips, 2005). It alludes to the importance of considering changes in

subsurface hydrological flows associated with shifts in vegetation types and measuring rooting characteristics. This is particularly relevant as we assess the effects of climate change, land cover and elevated atmosphere CO_2 concentrations on chemical weathering and carbon cycles.

570 *Data availability.* All data used for model parameterization can be acquired from http://lter.konza.ksu.edu/data. The input files necessary to reproduce the results are available from the authors upon request (lili@engr.psu.edu).

Author contributions. H. Wen, P. Sullivan and L. Li initiated the idea and designed the numerical experiments. G.L. Macpherson and S. Billings provided the field data. H. Wen ran the simulations, analyzed simulation results, and wrote the first draft of the manuscript. All co-authors participated in editing the manuscript.

575 *Competing interests.* The authors report no conflicts of interest.

Acknowledgement. We acknowledge funding support from the Konza Prairie LTER program (NSF DEB-1440484), the Signals in the Soils (SitS, EAR–1331726), and the NSF project (EAR-1911960). We appreciate the assistance of the Konza Prairie Biological Station. We are grateful for the field data provided by Misha Tsypin and Dr. Zachary Brecheisen.

References

580 Abongwa, P. T., and Atekwana, E. A.: Controls on the chemical and isotopic composition of carbonate springs during evolution to saturation with respect to calcite, Chem Geol, 404, 136-149, 10.1016/j.chemgeo.2015.03.024, 2015.
Ahrens, B., Braakhekke, M. C., Guggenberger, G., Schrumpf, M., and Reichstein, M.: Contribution of sorption, DOC transport and microbial interactions to the C-14 age of a soil organic carbon profile: Insights from a calibrated process model, Soil Biology & Biochemistry, 88, 390-402, 10.1016/j.soilbio.2015.06.008, 2015.
585 Andrews, J. A., and Schlesinger, W. H.: Soil CO2 dynamics, acidification, and chemical weathering in a temperate forest with experimental CO2 enrichment, Global Biogeochemical Cycles, 15, 149-162, 10.1029/2000gb001278, 2001.
Angers, D. A., and Caron, J.: Plant-induced changes in soil structure: Processes and feedbacks, Biogeochemistry, 42, 55-72, 10.1023/a:1005944025343, 1998.
Aragao, L., Malhi, Y., Metcalfe, D. B., Silva-Espejo, J. E., Jimenez, E., Navarrete, D., Almeida, S., Costa, A. C. L., Salinas, N.,
590 Phillips, O. L., Anderson, L. O., Alvarez, E., Baker, T. R., Goncalvez, P. H., Huaman-Ovalle, J., Mamani-Solorzano, M., Meir, P., Monteagudo, A., Patino, S., Penuela, M. C., Prieto, A., Quesada, C. A., Rozas-Davila, A., Rudas, A., Silva, J. A., and Vasquez, R.: Above- and below-ground net primary productivity across ten Amazonian forests on contrasting soils, Biogeosciences, 6, 2759-2778, 10.5194/bg-6-2759-2009, 2009.
Archer, D., and Brovkin, V.: The millennial atmospheric lifetime of anthropogenic CO2, Clim. Change, 90, 283-297,
595 10.1007/s10584-008-9413-1, 2008.
Beerling, D. J., Chaloner, W. G., Woodward, F. I., and Berner, R. A.: The carbon cycle and carbon dioxide over Phanerozoic time: the role of land plants, Philosophical Transactions of the Royal Society of London. Series B: Biological Sciences, 353, 75-82, doi:10.1098/rstb.1998.0192, 1998.
Bengtson, P., and Bengtsson, G.: Rapid turnover of DOC in temperate forests accounts for increased CO2 production at elevated
600 temperatures, Ecology letters, 10, 783-790, DOI: 10.1111/j.1461-0248.2007.01072.x, 2007.
Berner, E. K., and Berner, R. A.: Global environment: water, air, and geochemical cycles, Princeton University Press, 2012.
Berner, R. A.: Weathering, plants, and the long-term carbon cycle, Geochimica et Cosmochimica Acta, 56, 3225-3231, 10.1016/0016-7037(92)90300-8, 1992.
Berner, R. A.: Paleoclimate - The rise of plants and their effect on weathering and atmospheric CO2, Science, 276, 544-546,
605 10.1126/science.276.5312.544, 1997.
Beven, K., and Germann, P.: Macropores and water flow in soils revisited, Water Resour Res, 49, 3071-3092, 10.1002/wrcr.20156, 2013.

Billings, S. A., Hirmas, D., Sullivan, P. L., Lehmeier, C. A., Bagchi, S., Min, K., Brecheisen, Z., Hauser, E., Stair, R., Flournoy, R., and Richter, D. D.: Loss of deep roots limits biogenic agents of soil development that are only partially restored by decades
610   of forest regeneration, Elementa-Science of the Anthropocene, 6, 10.1525/elementa.287, 2018.
Brantley, S. L., Eissenstat, D. M., Marshall, J. A., Godsey, S. E., Balogh-Brunstad, Z., Karwan, D. L., Papuga, S. A., Roering, J., Dawson, T. E., Evaristo, J., Chadwick, O., McDonnell, J. J., and Weathers, K. C.: Reviews and syntheses: on the roles trees play in building and plumbing the critical zone, Biogeosciences, 14, 5115-5142, 10.5194/bg-14-5115-2017, 2017a.
Brantley, S. L., Lebedeva, M. I., Balashov, V. N., Singha, K., Sullivan, P. L., and Stinchcomb, G.: Toward a conceptual model
615   relating chemical reaction fronts to water flow paths in hills, Geomorphology, 277, 100-117, 10.1016/j.geomorph.2016.09.027, 2017b.
Breecker, D. O., Sharp, Z. D., and McFadden, L. D.: Atmospheric CO_2 concentrations during ancient greenhouse climates were similar to those predicted for AD 2100, Proceedings of the National Academy of Sciences of the United States of America, 107, 576-580, 10.1073/pnas.0902323106, 2010.
620   Brunner, I., Herzog, C., Dawes, M. A., Arend, M., and Sperisen, C.: How tree roots respond to drought, Frontiers in plant science, 6, 547, doi.org/10.3389/fpls.2015.00547, 2015.
Calmels, D., Gaillardet, J., and Francois, L.: Sensitivity of carbonate weathering to soil CO_2 production by biological activity along a temperate climate transect, Chem Geol, 390, 74-86, 10.1016/j.chemgeo.2014.10.010, 2014.
Canadell, J., Jackson, R. B., Ehleringer, J. R., Mooney, H. A., Sala, O. E., and Schulze, E. D.: Maximum rooting depth of
625   vegetation types at the global scale, Oecologia, 108, 583-595, 10.1007/bf00329030, 1996.
Carey, J. C., Tang, J. W., Templer, P. H., Kroeger, K. D., Crowther, T. W., Burton, A. J., Dukes, J. S., Emmett, B., Frey, S. D., Heskel, M. A., Jiang, L., Machmuller, M. B., Mohan, J., Panetta, A. M., Reich, P. B., Reinsch, S., Wang, X., Allison, S. D., Bamminger, C., Bridgham, S., Collins, S. L., De Dato, G., Eddy, W. C., Enquist, B. J., Estiarte, M., Harte, J., Henderson, A., Johnson, B. R., Larsen, K. S., Luo, Y., Marhan, S., Melillo, J. M., Peuelas, J., Pfeifer-Meister, L., Poll, C., Rastetter, E.,
630   Reinmann, A. B., Reynolds, L. L., Schmidt, I. K., Shaver, G. R., Strong, A. L., Suseela, V., and Tietema, A.: Temperature response of soil respiration largely unaltered with experimental warming, Proceedings of the National Academy of Sciences of the United States of America, 113, 13797-13802, 10.1073/pnas.160536511, 2016.
Cerling, T. E.: The stable isotopic composition of modern soil carbonate and its relationship to climate, Earth Planet Sc Lett, 71, 229-240, 10.1016/0012-821x(84)90089-x, 1984.
635   Cheng, J. H., Zhang, H. J., Wang, W., Zhang, Y. Y., and Chen, Y. Z.: Changes in Preferential Flow Path Distribution and Its Affecting Factors in Southwest China, Soil Science, 176, 652-660, 10.1097/SS.0b013e31823554ef, 2011.
Cole, J. J., Prairie, Y. T., Caraco, N. F., McDowell, W. H., Tranvik, L. J., Striegl, R. G., Duarte, C. M., Kortelainen, P., Downing, J. A., Middelburg, J. J., and Melack, J.: Plumbing the global carbon cycle: Integrating inland waters into the terrestrial carbon budget, Ecosystems, 10, 171-184, 10.1007/s10021-006-9013-8, 2007.
640   Costa, A.: Permeability‐porosity relationship: A reexamination of the Kozeny‐Carman equation based on a fractal pore‐space geometry assumption, Geophys Res Lett, 33, 10.1029/2005GL025134, 2006.
Covington, M. D., Gulley, J. D., and Gabrovsek, F.: Natural variations in calcite dissolution rates in streams: Controls, implications, and open questions, Geophys Res Lett, 42, 2836-2843, 10.1002/2015gl063044, 2015.
Dandurand, J. L., Gout, R., Hoefs, J., Menschel, G., Schott, J., and Usdowski, E.: Kinetically controlled variations of major
645   components and carbon and oxygen isotopes in a calcite-precipitating spring, Chem Geol, 36, 299-315, 10.1016/0009-2541(82)90053-5, 1982.
Deng, H., Voltolini, M., Molins, S., Steefel, C., DePaolo, D., Ajo-Franklin, J., and Yang, L.: Alteration and Erosion of Rock Matrix Bordering a Carbonate-Rich Shale Fracture, Environmental Science & Technology, 51, 8861-8868, 10.1021/acs.est.7b02063, 2017.
650   Drever, J. I.: The effect of land plants on weathering rates of silicate minerals, Geochim Cosmochim Ac, 58, 2325-2332, 10.1016/0016-7037(94)90013-2, 1994.
Eberbach, P. L.: The eco-hydrology of partly cleared, native ecosystems in southern Australia: a review, Plant and Soil, 257, 357-369, 10.1023/A:1027392703312, 2003.
Fan, Y., Miguez-Macho, G., Jobbagy, E. G., Jackson, R. B., and Otero-Casal, C.: Hydrologic regulation of plant rooting depth,
655   Proceedings of the National Academy of Sciences of the United States of America, 114, 10572-10577, 10.1073/pnas.1712381114, 2017.
Frank, D. A., Pontes, A. W., Maine, E. M., Caruana, J., Raina, R., Raina, S., and Fridley, J. D.: Grassland root communities: species distributions and how they are linked to aboveground abundance, Ecology, 91, 3201-3209, 10.1890/09-1831.1, 2010.
Gaillardet, J., Calmels, D., Romero-Mujalli, G., Zakharova, E., and Hartmann, J.: Global climate control on carbonate
660   weathering intensity, Chem Geol, 527, 118762, 10.1016/j.chemgeo.2018.05.009, 2019.
Gill, R. A., Kelly, R. H., Parton, W. J., Day, K. A., Jackson, R. B., Morgan, J. A., Scurlock, J. M. O., Tieszen, L. L., Castle, J. V., Ojima, D. S., and Zhang, X. S.: Using simple environmental variables to estimate below-ground productivity in grasslands, Global Ecology and Biogeography, 11, 79-86, 10.1046/j.1466-822X.2001.00267.x, 2002.
Goddéris, Y., Williams, J. Z., Schott, J., Pollard, D., and Brantley, S. L.: Time evolution of the mineralogical composition of
665   Mississippi Valley loess over the last 10 kyr: Climate and geochemical modeling, Geochimica Et Cosmochimica Acta, 74, 6357-6374, 10.1016/j.gca.2010.08.023, 2010.

Gupta, A., Rico-Medina, A., and Cano-Delgado, A. I.: The physiology of plant responses to drought, Science, 368, 266-269, 10.1126/science.aaz7614, 2020.

Harman, C. J., and Cosans, C. L.: A low-dimensional model of bedrock weathering and lateral flow coevolution in hillslopes: 2.
670   Controls on weathering and permeability profiles, drainage hydraulics, and solute export pathways, Hydrological Processes, 33, 1168-1190, 10.1002/hyp.13385, 2019.

Harper, C. W., Blair, J. M., Fay, P. A., Knapp, A. K., and Carlisle, J. D.: Increased rainfall variability and reduced rainfall amount decreases soil CO2 flux in a grassland ecosystem, Global Change Biology, 11, 322-334, 10.1111/j.1365-2486.2005.00899.x, 2005.

675   Hartmann, A., Goldscheider, N., Wagener, T., Lange, J., and Weiler, M.: Karst water resources in a changing world: Review of hydrological modeling approaches, Rev. Geophys., 52, 218-242, doi:10.1002/2013RG000443, 2014.

Hasenmueller, E. A., Jin, L. X., Stinchcomb, G. E., Lin, H., Brantley, S. L., and Kaye, J. P.: Topographic controls on the depth distribution of soil CO2 in a small temperate watershed, Appl Geochem, 63, 58-69, 10.1016/j.apgeochem.2015.07.005, 2015.

Hasenmueller, E. A., Gu, X., Weitzman, J. N., Adams, T. S., Stinchcomb, G. E., Eissenstat, D. M., Drohan, P. J., Brantley, S. L.,
680   and Kaye, J. P.: Weathering of rock to regolith: The activity of deep roots in bedrock fractures, Geoderma, 300, 11-31, 10.1016/j.geoderma.2017.03.020, 2017.

Heimann, M., and Reichstein, M.: Terrestrial ecosystem carbon dynamics and climate feedbacks, Nature, 451, 289-292, 10.1038/nature06591, 2008.

Houghton, R. A.: Balancing the global carbon budget, Annual Review of Earth and Planetary Sciences, 35, 313-347,
685   10.1146/annurev.earth.35.031306.140057, 2007.

Huang, F., Zhang, C. L., Xie, Y. C., Li, L., and Cao, J. H.: Inorganic carbon flux and its source in the karst catchment of Maocun, Guilin, China, Environmental Earth Sciences, 74, 1079-1089, 10.1007/s12665-015-4478-4, 2015.

Jackson, R. B., Canadell, J., Ehleringer, J. R., Mooney, H. A., Sala, O. E., and Schulze, E. D.: A global analysis of root distributions for terrestrial biomes, Oecologia, 108, 389-411, 10.1007/bf00333714, 1996.

690   Jiang, H., Deng, Q., Zhou, G., Hui, D., Zhang, D., Liu, S., Chu, G., and Li, J.: Responses of soil respiration and its temperature/moisture sensitivity to precipitation in three subtropical forests in southern China, Biogeosciences, 10, 3963-3982, 10.5194/bg-10-3963-2013, 2013.

Jobbagy, E. G., and Jackson, R. B.: The vertical distribution of soil organic carbon and its relation to climate and vegetation, Ecological Applications, 10, 423-436, 10.2307/2641104, 2000.

695   Kanduc, T., Mori, N., Kocman, D., Stibilj, V., and Grassa, F.: Hydrogeochemistry of Alpine springs from North Slovenia: Insights from stable isotopes, Chem Geol, 300, 40-54, 10.1016/j.chemgeo.2012.01.012, 2012.

Knapp, A., and Ojima, D.: NPP Grassland: Konza Prairie, USA, 1984-1990, R1, ORNL DAAC, 2014.

Kozeny, J.: Uber kapillare leitung der wasser in boden, Royal Academy of Science, Vienna, Proc. Class I, 136, 271-306, 1927.

Lawrence, C., Harden, J., and Maher, K.: Modeling the influence of organic acids on soil weathering, Geochim Cosmochim Ac,
700   139, 487-507, 10.1016/j.gca.2014.05.003, 2014.

Lebedeva, M. I., and Brantley, S. L.: Exploring geochemical controls on weathering and erosion of convex hillslopes: beyond the empirical regolith production function, Earth Surface Processes and Landforms, 38, 1793-1807, 10.1002/esp.3424, 2013.

Lett, M. S., Knapp, A. K., Briggs, J. M., and Blair, J. M.: Influence of shrub encroachment on aboveground net primary productivity and carbon and nitrogen pools in a mesic grassland, Canadian Journal of Botany-Revue Canadienne De Botanique,
705   82, 1363-1370, 10.1139/b04-088, 2004.

Li, L., Bao, C., Sullivan, P. L., Brantley, S., Shi, Y. N., and Duffy, C.: Understanding watershed hydrogeochemistry: 2. Synchronized hydrological and geochemical processes drive stream chemostatic behavior, Water Resour Res, 53, 2346-2367, 10.1002/2016wr018935, 2017.

Li, Y., Wang, Y. G., Houghton, R. A., and Tang, L. S.: Hidden carbon sink beneath desert, Geophys Res Lett, 42, 5880-5887,
710   10.1002/2015gl064222, 2015.

Lopez-Chicano, M., Bouamama, M., Vallejos, A., and Pulido-Bosch, A.: Factors which determine the hydrogeochemical behaviour of karstic springs. A case study from the Betic Cordilleras, Spain, Appl Geochem, 16, 1179-1192, 10.1016/s0883-2927(01)00012-9, 2001.

Luyssaert, S., Schulze, E. D., Borner, A., Knohl, A., Hessenmoller, D., Law, B. E., Ciais, P., and Grace, J.: Old-growth forests as
715   global carbon sinks, Nature, 455, 213-215, 10.1038/nature07276, 2008.

Ma, J., Liu, R., Tang, L. S., Lan, Z. D., and Li, Y.: A downward CO2 flux seems to have nowhere to go, Biogeosciences, 11, 6251-6262, 10.5194/bg-11-6251-2014, 2014.

Macpherson, G., and Sullivan, P. L. J. C. G.: Dust, impure calcite, and phytoliths: Modeled alternative sources of chemical weathering solutes in shallow groundwater, Chem Geol, 527, 118871, 10.1016/j.chemgeo.2018.08.007, 2019.

720   Macpherson, G. L.: Hydrogeology of thin limestones: The Konza Prairie Long-Term Ecological Research Site, Northeastern Kansas, J Hydrol, 186, 191-228, 10.1016/s0022-1694(96)03029-6, 1996.

Macpherson, G. L., Roberts, J. A., Blair, J. M., Townsend, M. A., Fowle, D. A., and Beisner, K. R.: Increasing shallow groundwater CO2 and limestone weathering, Konza Prairie, USA, Geochimica Et Cosmochimica Acta, 72, 5581-5599, 10.1016/j.gca.2008.09.004, 2008.

725   Mazvimavi, D., Meijerink, A. M. J., and Stein, A.: Prediction of base flows from basin characteristics: a case study from Zimbabwe, Hydrological Sciences Journal-Journal Des Sciences Hydrologiques, 49, 703-715, 10.1623/hysj.49.4.703.54428, 2004.

Moral, F., Cruz-Sanjulian, J. J., and Olias, M.: Geochemical evolution of groundwater in the carbonate aquifers of Sierra de Segura (Betic Cordillera, southern Spain), J Hydrol, 360, 281-296, 10.1016/j.jhydrol.2008.07.012, 2008.

730   Moriasi, D. N., Arnold, J. G., Van Liew, M. W., Bingner, R. L., Harmel, R. D., and Veith, T. L.: Model evaluation guidelines for systematic quantification of accuracy in watershed simulations, Transactions of the Asabe, 50, 885-900, 10.13031/2013.23153, 2007.

Mottershead, D. N., Baily, B., Collier, P., and Inkpen, R. J.: Identification and quantification of weathering by plant roots, Building and Environment, 38, 1235-1241, 10.1016/s0360-1323(03)00080-5, 2003.

735   Nardini, A., Casolo, V., Dal Borgo, A., Savi, T., Stenni, B., Bertoncin, P., Zini, L., and McDowell, N. G.: Rooting depth, water relations and non-structural carbohydrate dynamics in three woody angiosperms differentially affected by an extreme summer drought, Plant Cell and Environment, 39, 618-627, 10.1111/pce.12646, 2016.

Neff, J. C., and Hooper, D. U.: Vegetation and climate controls on potential CO_2, DOC and DON production in northern latitude soils, Glob. Change Biol., 8, 872-884, 10.1046/j.1365-2486.2002.00517.x, 2002.

740   Nepstad, D. C., Decarvalho, C. R., Davidson, E. A., Jipp, P. H., Lefebvre, P. A., Negreiros, G. H., Dasilva, E. D., Stone, T. A., Trumbore, S. E., and Vieira, S.: The role of deep roots in the hydrological and carbon cycles of amazonian forests and pastures, Nature, 372, 666-669, 10.1038/372666a0, 1994.

Nippert, J. B., Wieme, R. A., Ocheltree, T. W., and Craine, J. M.: Root characteristics of C-4 grasses limit reliance on deep soil water in tallgrass prairie, Plant and Soil, 355, 385-394, 10.1007/s11104-011-1112-4, 2012.

745   Noguchi, S., Tsuboyama, Y., Sidle, R. C., and Hosoda, I.: Spatially distributed morphological characteristics of macropores in forest soils of Hitachi Ohta Experimental Watershed, Japan, Journal of Forest Research, 2, 207-215, 10.1007/BF02348317, 1997.

Oades, J. M.: The role of biology in the formation, stabilization and degradation of soil structure, Geoderma, 56, 377-400, 10.1016/0016-7061(93)90123-3, 1993.

Ozkul, M., Gokgoz, A., and Horvatincic, N.: Depositional properties and geochemistry of Holocene perched springline tufa
750   deposits and associated spring waters: a case study from the Denizli Province, Western Turkey, in: Tufas and Speleothems: Unravelling the Microbial and Physical Controls, edited by: Pedley, H. M., and Rogerson, M., Geological Society Special Publication, 245-262, 2010.

Palandri, J. L., and Kharaka, Y. K.: A compilation of rate parameters of water-mineral interaction kinetics for application to geochemical modeling, Geological Survey Menlo Park CA, 2004.

755   Patrick, L., Cable, J., Potts, D., Ignace, D., Barron-Gafford, G., Griffith, A., Alpert, H., Van Gestel, N., Robertson, T., Huxman, T. E., Zak, J., Loik, M. E., and Tissue, D.: Effects of an increase in summer precipitation on leaf, soil, and ecosystem fluxes of CO_2 and H_2O in a sotol grassland in Big Bend National Park, Texas, Oecologia, 151, 704-718, 10.1007/s00442-006-0621-y, 2007.

Pawlik, L., Phillips, J. D., and Samonil, P.: Roots, rock, and regolith: Biomechanical and biochemical weathering by trees and its
760   impact on hillslopes-A critical literature review, Earth-Sci Rev, 159, 142-159, 10.1016/j.earscirev.2016.06.002, 2016.

Pennell, K. D., Boyd, S. A., and Abriola, L. M.: Surface-area of soil organic-matter reexamined, Soil Science Society of America Journal, 59, 1012-1018, 10.2136/sssaj1995.03615995005900040008x, 1995.

Phillips, J. D.: Weathering instability and landscape evolution, Geomorphology, 67, 255-272, 10.1016/j.geomorph.2004.06.012, 2005.

765   Plummer, L., Wigley, T., and Parkhurst, D.: The kinetics of calcite dissolution in CO 2-water systems at 5 degrees to 60 degrees C and 0.0 to 1.0 atm CO 2, Am J Sci, 278, 179-216, 10.2475/ajs.278.2.179, 1978.

Price, K.: Effects of watershed topography, soils, land use, and climate on baseflow hydrology in humid regions: A review, Progress in Physical Geography, 35, 465-492, 10.1177/0309133311402714, 2011.

Renard, P., and Allard, D.: Connectivity metrics for subsurface flow and transport, Adv Water Resour, 51, 168-196,
770   10.1016/j.advwatres.2011.12.001, 2013.

Richter, D. D., and Billings, S. A.: 'One physical system': Tansley's ecosystem as Earth's critical zone, New Phytol., 206, 900-912, 10.1111/nph.13338, 2015.

Romero-Mujalli, G., Hartmann, J., and Börker, J.: Temperature and CO_2 dependency of global carbonate weathering fluxes– Implications for future carbonate weathering research, Chem Geol, 527, 118874, 10.1016/j.chemgeo.2018.08.010, 2019a.

775   Romero-Mujalli, G., Hartmann, J., Börker, J., Gaillardet, J., and Calmels, D.: Ecosystem controlled soil-rock pCO_2 and carbonate weathering–Constraints by temperature and soil water content, Chem Geol, 527, 118634, 10.1016/j.chemgeo.2018.01.030, 2019b.

Steefel, C. I., Appelo, C. A. J., Arora, B., Jacques, D., Kalbacher, T., Kolditz, O., Lagneau, V., Lichtner, P. C., Mayer, K. U., Meeussen, J. C. L., Molins, S., Moulton, D., Shao, H., Šimůnek, J., Spycher, N., Yabusaki, S. B., and Yeh, G. T.: Reactive
780   transport codes for subsurface environmental simulation, Computational Geosciences, 19, 445-478, 10.1007/s10596-014-9443-x, 2015.

Stevens, N., Lehmann, C. E. R., Murphy, B. P., and Durigan, G.: Savanna woody encroachment is widespread across three continents, Glob. Change Biol., 23, 235-244, 10.1111/gcb.13409, 2017.

Steward, D. R., Yang, X., Lauwo, S. Y., Staggenborg, S. A., Macpherson, G. L., and Welch, S. M.: From precipitation to
785   groundwater baseflow in a native prairie ecosystem: a regional study of the Konza LTER in the Flint Hills of Kansas, USA,
       Hydrol Earth Syst Sc, 15, 3181-3194, 10.5194/hess-15-3181-2011, 2011.
       Sullivan, P. L., Stops, M. W., Macpherson, G. L., Li, L., Hirmas, D. R., and Dodds, W. K.: How landscape heterogeneity
       governs stream water concentration-discharge behavior in carbonate terrains (Konza Prairie, USA), Chem. Geol., 527, 118989,
       10.1016/j.chemgeo.2018.12.002, 2019.
790   Tsypin, M., and Macpherson, G. L.: The effect of precipitation events on inorganic carbon in soil and shallow groundwater,
       Konza Prairie LTER Site, NE Kansas, USA, Applied Geochemistry, 27, 2356-2369, 10.1016/j.apgeochem.2012.07.008, 2012.
       Vargas, R., Collins, S. L., Thomey, M. L., Johnson, J. E., Brown, R. F., Natvig, D. O., and Friggens, M. T.: Precipitation
       variability and fire influence the temporal dynamics of soil CO2 efflux in an arid grassland, Glob. Change Biol., 18, 1401-1411,
       10.1111/j.1365-2486.2011.02628.x, 2012.
795   Vergani, C., and Graf, F.: Soil permeability, aggregate stability and root growth: a pot experiment from a soil bioengineering
       perspective, Ecohydrology, 9, 830-842, 10.1002/eco.1686, 2016.
       Wang, J. A., Sulla-Menashe, D., Woodcock, C. E., Sonnentag, O., Keeling, R. F., and Friedl, M. A.: Extensive land cover
       change across Arctic-Boreal Northwestern North America from disturbance and climate forcing, Glob. Change Biol., 26, 807-
       822, 10.1111/gcb.14804, 2020.
800   Watson, K. W., and Luxmoore, R. J.: Estimating macroporosity in a forest watershed by use of a tension infiltrometer, Soil
       Science Society of America Journal, 50, 578-582, 10.2136/sssaj1986.03615995005000030007x, 1986.
       Weiler, M., and Naef, F.: An experimental tracer study of the role of macropores in infiltration in grassland soils, Hydrological
       Processes, 17, 477-493, 10.1002/hyp.1136, 2003.
       Wen, H., Li, L., Crandall, D., and Hakala, A.: Where lower calcite abundance creates more alteration: enhanced rock matrix
805   diffusivity induced by preferential dissolution, Energy Fuels, 30, 4197-4208, 10.1021/acs.energyfuels.5b02932, 2016.
       Wen, H., and Li, L.: An upscaled rate law for magnesite dissolution in heterogeneous porous media, Geochim Cosmochim Ac,
       210, 289-305, 10.1016/j.gca.2017.04.019, 2017.
       Wen, H., and Li, L.: An upscaled rate law for mineral dissolution in heterogeneous media: The role of time and length scales,
       Geochim Cosmochim Ac, 235, 1-20, 10.1016/j.gca.2018.04.024, 2018.
810   Wen, H., Perdrial, J., Abbott, B. W., Bernal, S., Dupas, R., Godsey, S. E., Harpold, A., Rizzo, D., Underwood, K., Adler, T.,
       Sterle, G., and Li, L.: Temperature controls production but hydrology regulates export of dissolved organic carbon at the
       catchment scale, Hydrol Earth Syst Sc, 24, 945-966, 10.5194/hess-24-945-2020, 2020.
       White, A. F., and Brantley, S. L.: The effect of time on the weathering of silicate minerals: why do weathering rates differ in the
       laboratory and field?, Chem Geol, 202, 479-506, 10.1016/j.chemgeo.2003.03.001, 2003.
815   Winnick, M. J., and Maher, K.: Relationships between CO2, thermodynamic limits on silicate weathering, and the strength of the
       silicate weathering feedback, Earth Planet Sc Lett, 485, 111-120, 10.1016/j.epsl.2018.01.005, 2018.
       Wolery, T. J., Jackson, K. J., Bourcier, W. L., Bruton, C. J., Viani, B. E., Knauss, K. G., and Delany, J. M.: Current Status of the
       Eq3/6 Software Package for Geochemical Modeling, Acs Sym Ser, 416, 104-116, 1990.
       Wu, Z. T., Dijkstra, P., Koch, G. W., Penuelas, J., and Hungate, B. A.: Responses of terrestrial ecosystems to temperature and
820   precipitation change: a meta-analysis of experimental manipulation, Glob. Change Biol., 17, 927-942, 10.1111/j.1365-
       2486.2010.02302.x, 2011.
       Zhang, Y. H., Niu, J. Z., Yu, X. X., Zhu, W. L., and Du, X. Q.: Effects of fine root length density and root biomass on soil
       preferential flow in forest ecosystems, Forest Systems, 24, 10.5424/fs/2015241-06048, 2015.
       Zhi, W., Li, L., Dong, W. M., Brown, W., Kaye, J., Steefel, C. I., and Williams, K. H.: Distinct Source Water Chemistry Shapes
825   Contrasting Concentration - Discharge Patterns, Water Resour Res, 55, 4233-4251, 10.1029/2018wr024257, 2019.
       Zhou, X. H., Talley, M., and Luo, Y. Q.: Biomass, Litter, and Soil Respiration Along a Precipitation Gradient in Southern Great
       Plains, USA, Ecosystems, 12, 1369-1380, 10.1007/s10021-009-9296-7, 2009.